Large magnetocrystalline anisotropy in bilayer transition metal phases from first-principles full-potential calculations

P. Ravindran,[1,*] A. Kjekshus,[1] H. Fjellvåg,[1] P. James,[2] L. Nordström,[2] B. Johansson,[2] and O. Eriksson[2]
[1]*Department of Chemistry, University of Oslo, Box 1033, Blindern, N-0315 Oslo, Norway*
[2]*Condensed Matter Theory Group, Department of Physics, Uppsala University, Box 530, 75121 Uppsala, Sweden*
(Received 24 January 2000; revised manuscript received 21 June 2000; published 19 March 2001)

The computational framework of this study is based on the local-spin-density approximation with first-principles full-potential linear muffin-tin orbital calculations including orbital polarization (OP) correction. We have studied the magnetic anisotropy for a series of bilayer CuAu(I)-type materials such as FeX, MnX (X = Ni,Pd,Pt), CoPt, NiPt, MnHg, and MnRh in a ferromagnetic state using experimental structural parameters to understand the microscopic origin of magnetic-anisotropy energy (MAE) in magnetic multilayers. Except for MnRh and MnHg, all these phases show perpendicular magnetization. We have analyzed our results in terms of angular momentum-, spin- and site-projected density of states, magnetic-angular-momentum-projected density of states, orbital-moment density of states, and total density of states. The orbital-moment number of states and the orbital-moment anisotropy for FeX (X = Ni,Pd,Pt) are calculated as a function of band filling to study its effect on MAE. The total and site-projected spin and orbital moments for all these systems are calculated with and without OP when the magnetization is along or perpendicular to the plane. The results are compared with available experimental as well as theoretical results. Our calculations show that OP always enhances the orbital moment in these phases and brings them closer to experimental values. The changes in MAE are analyzed in terms of exchange splitting, spin-orbit splitting, and tetragonal distortion/crystal-field splitting. The calculated MAE is found to be in good agreement with experimental values when the OP correction is included. Some of the materials considered here show large magnetic anisotropy of the order of meV. In particular we found that MnPt will have a very large MAE if it could be stabilized in a ferromagnetic configuration. Our analysis indicates that apart from large spin-orbit interaction and exchange interaction from at least one of the constituents, a large crystal-field splitting originating from the tetragonal distortion is also a necessary condition for having large magnetic anisotropy in these materials. Our calculation predicts large orbital moment in the hard axis in the case of FePt, MnRh, and MnHg against expectation.

DOI: 10.1103/PhysRevB.63.144409 PACS number(s): 75.25.+z, 75.30.Cr, 75.30.Gw

I. INTRODUCTION

Ferromagnetic materials exhibit intrinsic ''easy'' and ''hard'' directions of the magnetization. This magnetic anisotropy is, both from a technological and fundamental point of view, one of the most important properties of magnetic materials. Depending on the type of application, materials with high, medium, or low magnetic anisotropy will be required, for respective application as, e.g., permanent magnets, information storage media or magnetic cores in transformers, and magnetic recording heads. Hence a better understanding of the microscopic origin of the magnetic anisotropy is necessary to tailor the properties of magnetic materials.

Generally, if a ferromagnetic material lacks a high degree of magnetocrystalline anisotropy in the bulk (e.g., bcc Fe), assuming that the structure is not greatly distorted by substrate-imposed strain, the moments will lie in the layer (film) plane so as to minimize the free energy of the system (i.e., the magnetization direction is determined by shape anisotropy). For some applications, an in-plane magnetization is desirable. For example, in-plane anisotropy is useful for longitudinal recording, magnetostrictive and inductive heads, and media for magnetic-field sensors (where a small anisotropy field is desired). On the other hand, to obtain perpendicular magnetic anisotropy (PMA) implies some means to overcome the shape anisotropy due to the magnetostatic energy that favors in-plane magnetization. Many potential applications of epitaxial ferromagnetic films on semiconductor substrates require a perpendicular component of the magnetization. Such a configuration would permit perpendicular magnetic recording or magnetooptical recording employing either the Faraday effect (in transmission) or the magnetooptic Kerr effect (in reflection) to rotate the plane of polarization of light propagating perpendicular to the substrate. Magnetic layers with strong PMA are of great interest for magnetooptic recording media with predicted performances of up to 300 Gbit/in^2, in comparison with present commercial hard disks that have storage densities around 2 Gbit/in^2.[1] Hence, the potential need for materials with higher perpendicular magnetocrystalline anisotropy than the current conventional cobalt alloys for future high-density recording media is well known.[2] Because the mechanisms responsible for PMA are so poorly understood, the search for new materials currently proceeds empirically. Hence, it is important to investigate the microscopic origin of magnetic anisotropy in detail in order to identify potential candidates.

Novel phenomena such as magnetocrystalline anisotropy, magnetooptical effects, magnetic circular dichroism etc. caused by strong coupling among spin, orbital, and lattice degrees of freedom are central issues in the physics of transition-metal compounds over the last few years. The energy required to alter the magnetization direction is called

the magnetocrystalline-anisotropy energy (MAE). van Vleck[3] suggested that the origin of this anisotropy is the interaction of the magnetization with the crystal lattice, i.e., the spin-orbit coupling. MAE in cubic $3d$-transition metals is a very small quantity of only a few μeV/atom (Refs. 4 and 5) that becomes enhanced to the order of meV/atom in magnetic multi-layers.[6,7,7–9] The enhancement in the magnetic anisotropy is believed to originate from the interface magnetism. Chappert and Bruno[10] have proposed that lattice-misfit strain may, via magnetostriction, contribute to the volume anisotropy in coherent structures. One of the interesting issues relating to the magnetism at interfaces is to understand what factors determine the preferred orientation of the magnetic moment relative to the crystallographic axes. Originally, Néel[11] discussed the large anisotropy within a pair-interaction model in which the reduced symmetry at the interface results in anisotropies that differ greatly from that of the bulk. In the itinerant electron model, the enhanced magnetocrystalline anisotropy due to the altered electronic structure[12,13] in a multilayer is considered to be the major cause for the observed PMA in Co- or Fe-based multilayer films. Thus a positive interface contribution to overcome the negative volume effect results in PMA in such phases.

Since the discovery of PMA in metallic overlayers and multilayers,[14,15], this phenomenon has been a subject of great interest, particularly with regard to its microscopic origin. Despite numerous experimental and theoretical studies, a full understanding of PMA has not yet been achieved. It is known that many kinds of noble metal/Co multilayers such as Pd/Co, Pt/Co, and Au/Co have large perpendicular anisotropy,[15] which depends on crystallographic orientation.[16] Especially Co- or Fe-based multilayer films prepared by alternate deposition of transition metal (Co or Fe) and nonmagnetic metal (Pd, Pt, Ag, Au, etc.) have been extensively investigated. Most of these materials have strong PMA when the thicknesses of transition metal layers were thinner than a few monolayers.[15,17–21] A multilayer consisting of alternating single atomic layers of magnetic and nonmagnetic elements is the low thickness limit of a magnetic multilayer and it may be called magnetic bilayer. With a suitable selection of nonmagnetic component one can tune the magnetic anisotropy and magnetooptical properties of magnetic bilayers. The phases considered in the present calculations are simple and have a bilayer nature. Hence, the investigation of these materials is expected to contribute to better understanding about MAE in ultrathin multilayers.

Among the thin films and superlattice systems exhibiting perpendicular magnetic anisotropy, the face centered tetragonal (fct) phases of binary alloys like CoPt, NiPt, FePd, and FePt with the CuAu(I)-type structure, have in recent years attracted great interest. These phases can be considered to consist of a monoatomic, chemically modulated superlattice of the two elements. When grown with the monoatomic layers parallel to the film plane, i.e., with the **c** axis of the fct unit cell perpendicular to the film, the material exhibits perpendicular magnetic anisotropy. Since the first observation of perpendicular magnetic anisotropy in CoPt multilayer films by Carcia,[22] considerable attention has been focused on such phases for potential use in perpendicular magnetic recording media. Further, the magnetocrystalline anisotropies of FePt and CoPt are among the highest reported in the literature[23] making them attractive base materials for future high-density magnetic recording media.[24,25]

TABLE I. Magnetic-ordering temperature, Curie or Néel (T_C or T_N) for selected CuAu(I)-type phases.

Compound	T_C or T_N (in K)	Magnetic state	Reference
CoPt	1100	Ferromagnetic	103
FeNi		Ferromagnetic	95
FePd	720	Ferromagnetic	88
FePt	446	Ferromagnetic	99
MnNi	1080	Antiferromagnetic	100
MnPd	825	Antiferromagnetic	101
MnPt		Antiferromagnetic	102
MnRh	185	Ferromagnetic	49
MnHg		Antiferromagnetic	104
Ni/Pt		Ferromagnetic	50

Stoichiometric intermetallic phase of manganese with Ni, Pd, and Pt are antiferromagnets with unexpected high Néel temperatures (T_N) and also the magnetic moment on Mn in these materials are larger than expected (see Table I). MnNi is a very interesting case with the highest (among the $3d$-metal alloys) T_N (1080 K), accompanied by a $3.8\mu_B$ magnetic moment on Mn. MnHg and MnRh are also experimentally found to exhibit antiferromagnetism. However, for simplicity we have assumed a ferromagnetic ground state for all these phases in our calculation. These model systems are studied from a fundamental point of view, in order to get a better understanding of the microscopic magnetic properties and their relation to PMA. Other ordered phases considered here have relatively high saturation magnetization, Curie temperature (T_C), and magnetocrystalline anisotropy. Hence, it is interesting to carry out systematic studies on these materials to understand the microscopic origin of their superior magnetic properties compared with the $3d$ elements themselves. This is, in fact, one of the main motivations for the present study. A possible explanation for large PMA in this class of materials through systematic exploration of their electronic structure can also identify potential candidates for practical applications. One of the aims of the present investigation is to search for trends in MAE as a function of spin-orbit coupling, exchange splitting or the band filling (number of valence electrons). Further, it is expected that the study on these bilayer materials may provide a better understanding of the importance of structural distortion, hybridization between magnetic and nonmagnetic materials, and thereby induced changes in the electronic structure on the magnetic anisotropy.

Magnetic anisotropy calculations for bulk Fe, Co, and Ni from first-principles spin-polarized relativistic band theory have been attempted.[26,27] These calculations show that because of its smallness (of the order μeV/atom), the magnetocrystalline anisotropy is a sensitive function of fine details of the electronic structure of a solid. Consequently, the results obtained depend strongly on the approximations made, the numerical techniques used, and whether they are con-

verged with respect to, e.g., the size of the basis set and the numerical integration in **k** space, etc. The anisotropy energy, caused by the spin-orbit interaction, is much smaller than other electronic energies. This makes predictions sensitive to subtle details of the Fermi surface. In any case, high numerical accuracy and convergences must be achieved despite the substantial loss of symmetry caused by the spin-orbit interaction. Thus, the computational requirements of a first-principles theory are demanding. Hence, so far it has been very hard to extract a satisfactory picture of MAE for the transition metals, both qualitatively and quantitatively. In the case of magnetic multilayers, MAE is much larger than that for the $3d$ elements themselves and as a result, reliable predictions from theoretical calculations can be made. Good agreement has been reached between first-principles calculated anisotropies and the corresponding experimental values in Co-based multilayers.[8,28] Although the bicomponent and multicomponent phases may have larger anisotropies, the comparison to theory may be plagued by defects. Moreover, for the multilayers the structures are not well characterized experimentally and the influence on MAE of the interface roughness and the strain resulting from lattice mismatches of the component materials are not known. Calculations of MAE for the phases considered here, for which the crystal structure is well known, will make the comparison between theory and experiment more proper. Most of the calculations on MAE (Ref. 28) for multilayer materials presented in the literature were based on the atomic sphere approximation (ASA) where spherical potentials in overlapping spheres are used to replace the actual effective potential of the lattice in combination with a minimal basis set. To our knowledge, so far no full-potential calculations have been performed for these bilayer materials to explain the experimentally observed large magnetic anisotropy. However, several attempts have been made[9,29–31] to estimate MAE for FePd, FePt, and CoPt from ASA methods that employed the force theorem. The reason for the lack of full-potential calculations for MAE in multilayers is that the calculations involved not only require high-precision total-energy methods, but also involve unduly large numbers of **k** points. It is demonstrated that the full-potential total-energy calculations based upon the local-density approximation of the density-functional theory in combination with an orbital-polarization correction can be used to derive the magnetocrystalline anisotropy energy for ferromagnetic metals.[27] We demonstrate here that the same approach can be extended to phases and multilayers that posses orders-of-magnitude higher MAE than the ferromagnetic metals.

The spin and orbital moments are basic quantities for magnets and their separate determination is very important in clarifying electronic structure and other physical properties. Until recently, experimental information on orbital moments has been available only for a very small number of systems, including the ferromagnetic $3d$ metals themselves, their alloys, and a few intermetallic phases. For some systems only average orbital moments are known, for example, those obtained from Einstein–de Hass experiments or ferromagnetic resonance. Atom-specific orbital moments have been measured in only a few cases, making use of spin-polarized neutron diffraction on single crystals. A recent development has been the theoretical[32] and experimental[33] progress in the field of x-ray magnetic circular dichroism (XMCD) as a chemically specific technique for probing orbital magnetism. There can be quite strong modifications of MAE as well as spin and orbital moments when a $3d$ element is substituted in a phase. Further, there is a strong connection between the anisotropy in the orbital moments and MAE for ferromagnetic materials. Hence, it is interesting to study in detail the origin of orbital moments in multilayer phases. It has been demonstrated that the orbital moments in magnetic materials can be reliably predicted if one includes orbital polarization (OP) correction into the local-spin-density approximation (LSDA) calculations.[34–37] So, we have calculated the orbital moments for a series of these phases and also as a function of band filling.

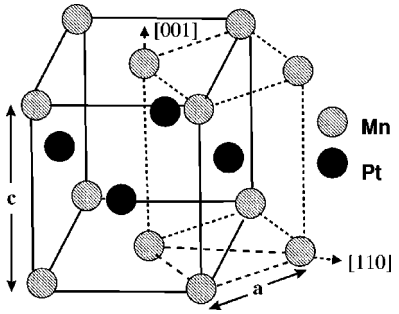

FIG. 1. Atomic arrangement in the CuAu(I)-type structure exemplified for MnPt. The spin quantization axes used in our MAE calculations are shown as dashed lines with arrows. The primitive tetragonal structure used in our calculations are represented by dotted lines.

The rest of this paper is organized as follows. Details about the CuAu(I)-type structure are given in Sec. II. After a brief discussion of how the anisotropy energy is calculated and other computational details in Sec. III, the angular momentum- and site-projected DOS, total DOS (TDOS), m_l-projected DOS (LDOS), orbital-moment density of states (ODOS), orbital-moment number of states (ONOS), and difference in the orbital-moment number of states (ΔONOS) are presented in Sec. V. The spin and orbital moments with and without OP correction and calculated MAE are compared with available experimental and theoretical values. On this basis, a detailed analysis of the anisotropy energy is presented and the importance of factors such as orbital-moment anisotropy (OMA), exchange splitting, spin-orbit splitting, crystal-field splitting, and band filling for obtaining a large PMA is discussed. Conclusions are summarized in Sec. VI.

II. STRUCTURAL ASPECTS

A particular structure obtained by stacking of alternating single-different atomic layers is the tetragonal CuAu(I)-type structure as shown in Fig. 1. The atomic-size difference between the two atom components is less than 15% for CuAu(I)-type phases, which indicates that the size factor is important for the stability of this structure. Importantly, re-

cent development of sophisticated growth techniques have made it possible to easily grow high-quality tetragonal CuAu(I)-type materials. In MnPt the stacking sequence along [001] consists of alternate Mn and Pt planes producing a tetragonal distortion along this direction. Along [100] and [110] the planes have equiatomic compositions. Each Mn atom is surrounded by eight Pt and four Mn (in plane) nearest neighbors, with local symmetry D_{4h}, as shown in Fig. 1. The unit cell contains four atoms, but can be expressed in terms of a simple tetragonal unit cell with two atoms, one at (0 0 0) and the other at $(\frac{1}{2}\frac{1}{2}\frac{1}{2})$ with $a=a_{\mathrm{CuAu}(I)}/\sqrt{2}$. For computational simplicity we chose to use the simple tetragonal structure with two atoms per primitive cell (dotted line in Fig. 1). This structure can be visualized as a tetragonally distorted version of the cubic CsCl-type structure. In this description, a c/a value of 1.0 corresponds to a body-centered-cubic lattice whereas $c/a=\sqrt{2}$ is equivalent to an fcc lattice. This relationship between fcc and bcc is often referred to as the Bain path. All the phases considered here have an axial ratio less than unity. This indicates that the bonding between unlike atoms is strong (i.e., strong interlayer bonding).

III. COMPUTATIONAL DETAILS

The calculations are based on a full-potential linear muffin-tin orbital method (FPLMTO) (Ref. 38) modified to be able to treat the MAE problem.[27] Since a total-energy calculation of this kind requires a tremendous energy resolution, some further details are given below. For computational purposes, the crystal is divided into nonoverlapping spheres surrounding atomic sites (muffin-tin spheres) where the density and potential vary rapidly, whereas in the interstitial regions between the spheres the density and potential vary slowly. In the muffin-tins (MT), the basis functions and electron density and potential are expanded in spherical waves; in the interstitial regions, they are expanded in Fourier series. In this method there is no shape approximation made for either the charge density or the potential; all electrons are involved in the self-consistent process and the core electrons are treated fully relativistically. The calculations include the effect of spin polarization within the local-spin-density approximation and spin-orbit coupling is included self consistently in the same way as have been previously reported for heavy elements and compounds.[35] The exchange-correlation potential is calculated with use of the von Barth–Hedin form. Lattice harmonics with angular momentum ℓ up to 8 are used to expand the charge and spin densities and wave functions inside the muffin-tin sphere. Moreover, the present calculations made use of a so-called multibasis to ensure a well-converged wave function. This means that several Hankel or Neumann functions depending on the sign of the kinetic energy of the basis function in the interstitial region have been used, each attached to its own radial function with an (n,ℓ) quantum number. Thus three *s*, two *p*, and three *d* orbitals appear in the expansion of the crystal wave function, each connecting to an envelope function with a unique kinetic energy for each atom. For the Brillouin zone integration (BZI) a Gaussian broadening method was used, which convolutes each discrete eigenvalue with a Gaussian function of width 10 meV. In these calculations the MT radii are kept as large as possible (without overlapping one another) which means that the muffin-tins fill about 65% of the total volume. In all cases a uniform mesh of **k** points is used, distributed as to fulfill the symmetry of the system for a particular direction of spin quantization.

Calculation of MAE requires resolving the difference in total energy (which often is of the order of several thousands of Ry) with accuracy some times better than 1 μRy when the magnetization is pointing in two different directions of the solid. Compared with the non-spin-polarized total-energy calculations, the numerical diagonalization procedure when calculating MAE is slower not only due to doubling of the Hamiltonian matrix by the spin polarization, but also by the reduction in the crystal symmetry by lifting of spin-degeneracy by spin-orbit interaction. Further, the reduction in symmetry makes the number of **k** points to be sampled larger in order to have a well-converged total energy. As mentioned earlier,[27,39] we have performed different convergence tests to ensure that the calculations have reached the required accuracy. Since the anisotropy energy arises primarily from the detailed electronic structure, especially energy-band structures in the regions near band crossings and electron states close to the Fermi energy, it is important to have a fine mesh of **k** points to obtain a realistic result. One of the problems one faces is that the sampling of the Brillouin zone (BZ) has to be performed with extreme care and the total energy needs to be converged with respect to the number of **k** points used for sampling the irreducible part of BZ. To illustrate this we show in Fig. 2 the calculated MAE as a function of the number of **k** points for XPt (X = Mn, Fe, Co, Ni). We notice that to achieve convergence in MAE with respect to the number of **k** points, about 10 000–15 000 **k** points in the full BZ is needed for these systems.

Orbital polarization and orbital moment

Since the spin-polarization and the relativistic spin-orbit interaction are taken into account in usual density-functional calculations, Hund's first and third rules, respectively, are taken into account in the normal LDA calculation. An exact formalism for including effects responsible for Hund's second rule is lacking at present. Hence, the calculated orbital moment in the systems is usually lower than the experimental values. From the analysis of experimental and theoretical MAE, Jansen[40] concluded that the energy density functional together with the spin-orbit coupling must contain terms that depend directly on the orbital moment. Based on van Vleck and Racha's vector model for atomic multiplets an approximate energy expression for Hund's second rule was derived.[34,36,41] The orbital-polarization energy for a particular spin-quantization direction $\hat{n}$ was found to be well approximated by

$$E_{OP}=-\frac{1}{2}\sum_{\sigma} BL_{z,\sigma}^{2}, \tag{1}$$

where B (for *d* states) is a Racah parameter[42] and $L_{z,\sigma}$ is the z component of the orbital angular momentum of σ-spin

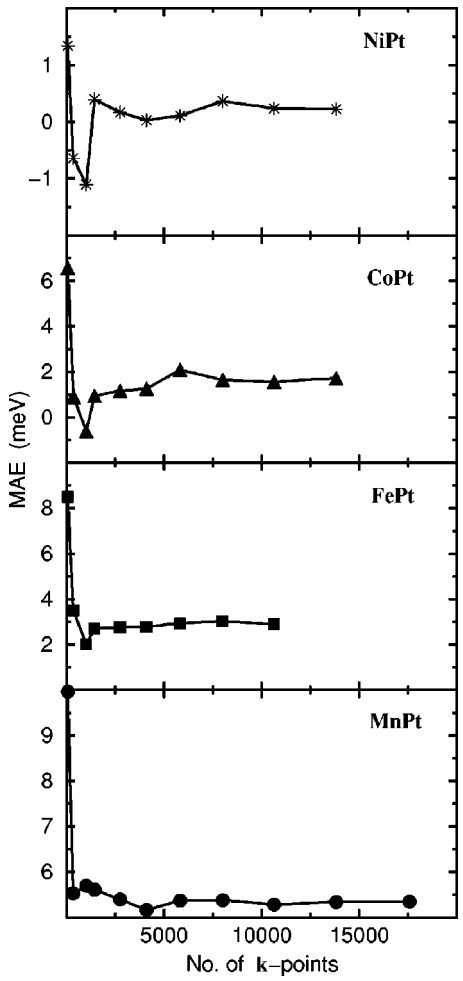

FIG. 2. Changes in magnetocrystalline-anisotropy energy (MAE) from SO+OP calculation for MPt (M=Mn, Fe, Co, Ni) as a function of total number of k points used in the whole Brillouin zone.

states (in the $\hat{n}$ direction). The parameter B can be expressed in terms of Slater integrals (F^2,F^4) of the single-particle wave functions for all d electrons and is recalculated for each iteration step from the relation[43]

$$B=\frac{9F^2-5F^4}{441}, \tag{2}$$

where the Slater F^k integrals are given by

$$F^k=\int\int \phi_d^2(r_1)\phi_d^2(r_2)\frac{2r_<^k}{r_>^{k+1}}r_1^2r_2^2dr_1dr_2. \tag{3}$$

For a crystal we replace the radial-wave function ϕ_d with the d partial wave evaluated at the center of gravity of the occupied part of the d band. The physical meaning of OP is that states with different angular momentum have different angular shape and hence a different Coulombic interaction, which are via Eq. (1) included in the energy functional. Applying this energy expression to solids one finds that it gives rise to energy shifts for the single-particle states with different magnetic quantum numbers. The OP term is included in the diagonal elements of the Hamiltonian matrix. Thus at each atom site, orbital polarization is allowed for by means of an eigenvalue shift, $\Delta V_{m_l}=-BL_zm_l$ that depends on the quantities obtained from the previous iteration step. The entire process is self-consistent and no parameters were adjusted. This means that the calculations incorporate all three Hund's rules (spin splitting, orbital splitting, and spin-orbit splitting) and, within the stated approximations, are fully self consistent. It is well known that LSDA calculations often give a too small orbital moment (by up to 50%) for, e.g., Fe and Co phases (see Ref. 44) and that the OP correction is a remedy for this defect in LSDA. This correction yielded larger orbital moments for Fe, Co, and Ni and thus a better agreement for the calculated g factors for Fe and Co with experiment.[36]

Just as the spin moment can be written as the expectation value of s_z one can calculate the orbital moment. The orbital magnetic moment on the Nth site is given by the expression[45]

$$\langle\hat{L}_z\rangle_N=\frac{\mu_B}{(2\pi)^3\Omega}\sum_i\int dk\langle ik|\hat{L}_z|ik\rangle_N, \tag{4}$$

where i refers to the occupied relativistic band states and the z projection of the orbital-moment operator $\hat{L}_z$, and Ω is the unit-cell volume. The expectation values $\langle ik|\hat{L}_z|ik\rangle_N$ are calculated within the Nth atomic site.

IV. CALCULATION OF MAE

The energy involved in rotating the magnetization from a direction of low energy toward one of high energy is called magnetic anisotropy. Various contributions to the magnetic anisotropy such as the magnetic dipolar, the magnetocrystalline, and the magnetostrictive contribution in multilayer films were recently reviewed.[21] The total anisotropy per monolayer in a magnetic multilayer can be written as

$$K^{tot}=K_v^{eff}+K_{shape}+\left(\frac{2K_s}{n_d}\right), \tag{5}$$

where $K_v^{eff}(=K_{mc}+K_{me})$ is the sum of the magnetocrystalline and magnetoelastic contributions, $K_{shape}=-2\pi M_s^2$, is the shape contribution for a uniform sheet of bulk material, and $2K_s$ is the anisotropy energy density from the two interfaces/surfaces for each magnetic layer and n_d is the number of atomic layers in the film. The surface/interface contribution to the anisotropy energy decreases with increasing multilayer thickness. In the majority of works only K_s is investigated while the K_v^{eff} term is argued to be small. The argument for neglecting K_v^{eff} is often based on the fact that MAE for thin films is much larger than that of the bulk crystal. The main origin of K_v^{eff} is the spin-orbit coupling.

In a quadratic approximation, for a uniaxial crystal like the tetragonal crystals considered in the present calculation, the magnetic anisotropy is described by[46]

$$E=K_1\sin^2\theta+K_2\sin^4\theta+K_2'\sin^4\theta\cos^4\phi+\cdots, \tag{6}$$

TABLE II. Unit-cell parameters (a and c in Å) and axial ratios for the primitive tetragonal unit cell used in the present calculations.

Compound	a	c	c/a
CoPt	2.6912	3.6839	1.3688
FeNi	2.5307	3.5789	1.4142
FePd	2.7294	3.7309	1.3669
FePt	2.7301	3.7879	1.3874
MnHg	3.2279	3.3129	1.0263
MnNi	2.6317	3.5294	1.3411
MnPd	2.8779	3.5899	1.2474
MnPt	2.8298	3.6647	1.2950
MnRh	2.7789	3.5599	1.2810
NiPt	2.7032	3.5889	1.3276

where K_1 is the second-order out-of-plane anisotropy constant and K_2 and K_2' are the fourth-order uniaxial and basal-plane anisotropy constants, respectively, θ the angle between the c axis and the magnetization vector, and ϕ is the azimuthal angle. Usually, the anisotropy within the plane (i.e., K_2 and K_2') is smaller than K_1 and we have considered only the second-order anisotropy constant in our calculations. Hence, we will define the magnetic anisotropy energy as the difference in the total energy when the magnetization is oriented along the plane, i.e., $\hat{n}=[110]$, and when it is oriented perpendicular to (001). Hence, in our definition of MAE a positive value means that the easy axis is along the c axis and the hard axis is in the **ab** plane. Using the full-potential LMTO method presented with the computational details given above we have calculated K_1 for the mentioned tetragonal CuAu(I)-type phases. In the calculations the experimental unitcell parameters given in Table II were used.

V. RESULTS AND DISCUSSION

MAE from spin-orbit (SO) and SO+OP calculations are given in Table III along with available experimental and theoretical values. It should be noted that for all phases the easy axis is correctly predicted, both with and without OP, but only fair agreement between the experimental and theoretical energies is obtained from SO calculations. The MAE is roughly doubled (except for NiPt) when OP is included, which moves the calculated values closer to the experimental ones. [001] is the easy direction for all compounds in Table III except MnHg and MnRh, for which the easy direction is along [110]. The experimental MAE for Fe, Co, and Ni are of the order of μeV/atom.[47] The binary layered materials studied here have an MAE of the order of meV/f.u. indicating that the magnetic anisotropy of the system may be enhanced by orders of magnitude in multicomponent systems by the proper selection of constituents.

Some of the experimentally observed magnetic properties of these materials are given in Table I. All the Mn phases considered in this paper are antiferromagnetic, however, it is worthwhile to note that ferromagnetic MnNi alloys have been grown with the easy axis of magnetization perpendicular to the layer plane.[48] Furthermore, the antiferromagnetic (AF) phase of MnRh transforms into a ferromagnetic one at low substitution levels of Bi or Te on the Rh site.[49] Possibly one may stabilize ferromagnetism also in the other AF phases by proper chemical substitution. For this reason it is highly interesting to perform calculations for the Mn-based AF phases in the ferromagnetic state. Our calculations show that NiPt possesses perpendicular anisotropy with large MAE. The established PMA in NiPt is consistent with recent experimental data in the sense that Ni/Pt multilayer films show PMA at room temperature.[50] Krishnan *et al.*[51] reported that Ni/Pt multilayers with Ni layers thinner than about 2 nm show perpendicular anisotropy and ferromagnetism. Table III shows that the Pd and Pt phases have large MAE. A possible reason is that both Pd and Pt have a large Stoner-enhanced susceptibility together with a large spin-orbit coupling. Thus they acquire a sizable spin-polarization in contact with $3d$ magnets and give an important contribution to the anisotropy, due to their large spin-orbit coupling. This viewpoint is supported by the observation[26] that suppression of the spin-orbit interaction in Pd reduces the calculated anisotropy of Pd/Co/Pd films. Our prediction of perpendicular

TABLE III. Calculated magnetic-anisotropy energies (MAE in meV) obtained from relativistic FPLMTO calculations without (SO) and with orbital-polarization corrections (SO+OP). The results are compared with experimental and other theoretical values.

Phase	SO	SO+OP	Theory (others)	Experiment	Easy axis
CoPt	1.052	1.642	1.50[a]	1.451	[001]
		1.782[b]		1.583[c]	[001]
				1.665[d]	[001]
				1.0[e]	[001]
FeNi	0.077	0.172		0.254	[001]
FePd	0.154	0.342	0.55[e]	0.5204[f]	[001]
				0.48[g]	[001]
				0.63[c]	[001]
				0.5898[h]	[001]
FePt	2.734	2.891	2.8[a]	0.8811[f]	[001]
		2.258[b]			[001]
		2.75[e]			[001]
MnHg	−0.068	−0.069			[110]
MnNi	0.023	0.116			[001]
MnPd	0.077	0.147			
MnPt	4.696	5.342			[001]
MnRh	−0.163	−0.285			[110]
NiPt	1.248	0.239			[001][i]

[a]Sakuma (Theory) (Ref. 29).
[b]Solovyev *et al.* (Theory) (Ref. 30).
[c]Maykov *et al.* (Experiment) (Ref. 88).
[d]Brissoneau *et al.* (Experiment) (Ref. 89).
[e]Oppeneer (Theory) (Ref. 31).
[f]Pyn'ko *et al.* (Experiment) (Ref. 90).
[g]Kamp *et al.* (Experiment) (Ref. 91).
[h]Magat *et al.* (Experiment) (Ref. 92).
[i]Kim and Shin (Experiment) (Ref. 50).

anisotropy in FeNi is consistent with experimental studies in the sense that the distribution function of the magnetic hyperfine fields of ultrathin Fe/Ni multilayers gives an out-of-plane anisotropy at the interface.[52] The increase in MAE from FeNi to FePt in Table III is due to enhancement of the spin-orbit splitting. The calculated MAE for NiPt is only 0.239 meV, much less than that for FePt, Table III. There is also a large difference in the calculated total magnetic moment in the easy magnetization direction, $3.41\mu_B$ for FePt and $0.66\mu_B$ for NiPt, respectively. The smaller value of MAE in NiPt compared to FePt is to some part the result of a weaker exchange splitting. Since the full-potential calculations have the most flexible basis set as well as a more exact effective potential, the results reported in Table III must be considered to be more accurate one that can be obtained from the density-functional calculation.

The present total-energy results refer to 0 K, whereas all measurements have been performed at finite temperature. Hence, the small difference between the experimental and theoretical MAE value is at least partly due to a temperature effect. Another reason for the larger MAE value in the theoretical studies is that the calculations are made for an ideally ordered lattice. Available experimental data for FePt show that the perpendicular magnetic anisotropy increases with the degree of layer ordering.[53]

Two types of contributions to the anisotropy energy can be distinguished.

(1) A contribution induced by the spin-orbit interaction causing splitting of partly occupied orbitally degenerate levels and resulting in a lowering of the total energy. Also, the spin-orbit interaction couples eigenstates ψ_i and ψ_j with energies ϵ_i below the Fermi energy and ϵ_j above the Fermi energy. Since the spin-orbit splitting depends on the magnetization direction, so does the total energy. If the spin-orbit coupling parameter ξ is sufficiently small, one can use perturbation theory to deduce the contribution to the anisotropy energy.

(2) Another contribution induced by crystal-field splitting is caused by the reduction in symmetry of the systems when going from cubic to lower symmetric structures.

These contributions are discussed in detail below. However, first we outline briefly the details of the calculated electronic structure, and spin and orbital moments, since this helps in understanding the analysis of MAE.

A. DOS characteristics

The spin-polarized total density of states for FePd and MnPd are shown in Fig. 3. For all these phases the valence band is mainly constituted by *d* bands. The profile of TDOS is structurally similar for all these phases: an almost completely occupied band of electrons with majority spin and the Fermi level (E_F) on the low-energy slope of the intense peak of DOS with minority spin. The topology of the TDOS of FePd and MnPd are similar. However, E_F is located so as to reflect the one-electron difference in the valence electrons between these two compounds. The rigid-band model seems to hold for the gross feature of DOS. A characteristic aspect

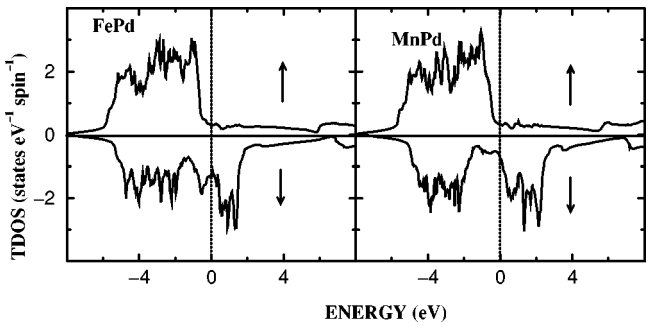

FIG. 3. Total density of states (TDOS) for FePd and MnPd phase obtained from SO+OP calculation.

commonly seen in these systems is that the *d* bands of Pd and Fe/Mn form bonding and antibonding states. In the minority spin state the *d* bands of Pd and Fe/Mn strongly overlap in the energy region near E_F. Similar to other ferromagnets, the width of the majority band is narrower than the minority band. The behavior of TDOS near E_F depends largely on the contribution of Fe $3d$ states in Fe*X* phases. The *d* bands of Pd and Pt are almost completely occupied independently of the magnetization direction.

In order to understand the role of the hybridization between the Fe and *X* atoms in the electronic structure of the Fe*X* phases, the site-, angular momentum-, and spin-projected density of states (PDOS) of Fe*X* phases are shown in Fig. 4. It is seen that the *d* states of the *X* atoms are energetically almost degenerate with the majority spin DOS of the Fe atom in the whole valence-band range, giving rise to substantial hybridization between Fe $3d^{\uparrow}$ and *X* $d^{\uparrow\downarrow}$ states. Further, the *d* bands of the *X* atoms are almost totally filled for both spin channels. In contrast to bulk Fe, the majority-spin $3d$ bands of Fe is completely filled due to the consequence of the band narrowing resulting from the enhancements of the Fe-Fe distance and this leads to an enhanced magnetic moment. The PDOS for FePt in Fig. 4 shows that the Pt $5d$ DOS has a peak structure just above E_F in the majority-spin state. This feature is not present in the Ni $3d$ or Pd $4d$ DOS in Fig. 4. Consistent with our findings, the XMCD spectra at the Pt $N_{6,7}$ edge in Fe/Pt multilayers indicate[54] that the Pt-$5d$ PDOS just above the Fermi level is higher for the majority-spin states than for the minority-spin states.

The $N(E_F)$ values are directly related to the electronic part of the specific-heat coefficient and calculated values of $N(E_F)$ are given in Table IV. The tabulated value of $N(E_F)$ for FePd is in good agreement with the experimental value of 18.3 states/(Ry f.u.) obtained from specific-heat measurements.[55] From the $N(E_F)$ values obtained from specific heat measurements on ordered and disordered FePd, Kuang *et al.*[55] concluded that a lower value of $N(E_F)$ for the ordered crystal structure relative to that of a disordered structure is due to the formation of a superlattice Brillouin zone. From PDOS for FePd in Fig. 4 it is clear that the small value of $N(E_F)$ is due to E_F lying on a pseudogap in the $3d^{\uparrow\downarrow}$ states of Fe and that the Pd $4d$ states have negligible contributions at E_F. Our calculated value of $N(E_F)$ for CoPt in Table IV agrees well with the value of 29.9 states/(Ry f.u.)

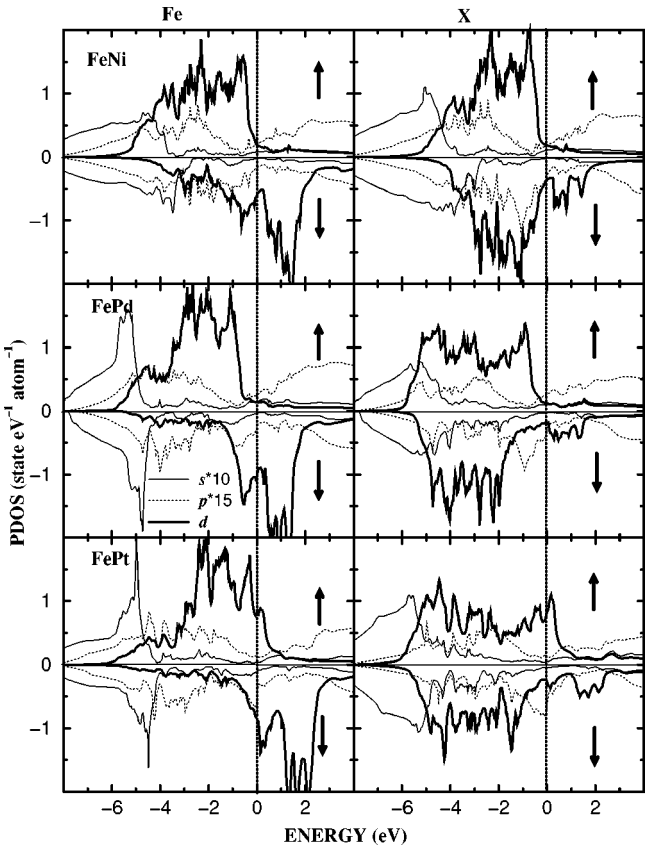

FIG. 4. Angular momentum-, spin-, and site-projected density of states (PDOS) for Fe*X* phases obtained from SO+OP calculations with the magnetic-quantization axis along [001]. The left panel represents PDOS for Fe and the right panel represents the PDOS for *X*. The ↑ symbol means majority-spin electrons, ↓ minority-spin electrons. For clarity the *s* and *p* states are scaled by factors 10 and 15, respectively. E_F is set to zero and represented by vertical dotted line.

obtained[56] from the ASA calculation. From specific-heat measurements[57] the electronic-specific-heat coefficient, $\gamma = 11.6$ mJ/(mol K^2) has been obtained for NiPt. The magnetic properties of many of these alloys are sensitive to the local atomic environment. For example, ordered NiPt is an antiferromagnetic phase[58] with low $N(E_F)$ whereas its disordered counterpart is ferromagnetic with large $N(_F)$.[59] For the remaining phases no electronic-specific-heat data are available. We hope that the presently reported $N(E_F)$ values in Table IV will motivate further experimental studies.

B. Spin and orbital moment

In Table IV we give the spin moments from SO+OP calculations, within each MT site and for the interstitial region, in all cases for the moments aligned along [001] or [110]. For comparison, available experimental (from magnetization, neutron diffraction, and XMCD measurements) and theoretical (from ASA calculations) values of spin and orbital moments are given in Table V. Our calculations show that the OP correction does not change the spin moment significantly although the orbital moment enhancement is almost 100%. Further, the fact that one derives almost the same spin moment for both magnetization directions indicates that the magnetic anisotropy is originating from the anisotropy of the orbital moment. The spin moments of Mn and Fe for the Pd-based phases are larger than for the Pt-based phases as can be seen from Table IV. This is a hybridization effect, where the large $5d$ overlap with the $3d$ orbitals reduces the moment.

TABLE IV. Calculated density of states at the Fermi level $[N(E_F)$ in states/(Ry f.u.)] site-projected spin moments obtained from relativistic FPLMTO calculation with orbital-polarization correction. Spin moments are denoted by the subscript *s*, and the total moment by *t*. **A** denotes the first atom site ($3d$ element), **B** denotes the second atom site, and ''Int'' means the interstitial region. All atomic moments are in units of μ_B/atom and the total moment in μ_B/f.u.

Phase	$N(E_F)$	$\mathbf{A}_s$	$\mathbf{B}_s$	Int_s	AB_s
CoPt [001]	21.025	1.803	0.394	−0.051	2.146
CoPt [110]	28.527	1.809	0.398	−0.051	2.156
FeNi [001]	18.215	2.568	0.679	−0.028	3.219
FeNi [110]	18.205	2.568	0.679	−0.028	3.219
FePd [001]	20.224	2.949	0.369	−0.042	3.276
FePd [110]	20.314	2.949	0.369	−0.042	3.277
FePt [001]	18.943	2.891	0.353	−0.039	3.205
FePt [110]	19.091	2.893	0.355	−0.039	3.209
MnHg [001]	34.062	3.671	−0.034	0.038	3.675
MnHg [110]	34.733	3.671	−0.034	0.038	3.675
MnNi [001]	39.048	3.100	0.581	0.061	3.742
MnNi [110]	39.074	3.098	0.580	0.061	3.739
MnPd [001]	13.514	3.798	0.356	0.151	4.305
MnPd [110]	13.643	3.798	0.356	0.151	4.305
MnPt [001]	20.569	3.620	0.338	0.067	4.025
MnPt [110]	22.487	3.613	0.335	0.066	4.014
MnRh [001]	36.572	3.066	0.065	0.061	3.192
MnRh [110]	36.314	3.066	0.062	0.061	3.189
NiPt [001]	44.793	0.426	0.199	−0.014	0.611
NiPt [110]	44.822	0.378	0.180	−0.013	0.545

In Fig. 4 the valence bands formed by the Fe $3d$ and *X* $3d$, $4d$, or $5d$ states in Fe*X* phases are displayed and a substantial exchange splitting between the spin-up and spin-down subbands is found on the Fe $3d$ states. As a result the Fe spin moment dominates whereas the *X* spin moment is much smaller. It is well known that the proximity of a nonmagnetic metal suppresses the magnetic moment of some elements depending on the extent of overlap between the *d* band of the magnetic metal and conduction band of the nonmagnetic metal. For the present systems, taking FePt as an example, the reduced number of Fe neareast neighbors narrows the bandwidth relative to that in pure Fe, which in turn increases the spin moment. However, compared to FePd the moment of FePt is smaller, since, as pointed out above, the $3d$-$5d$ overlap is larger than the $3d$-$4d$ overlap. In contrast, like for a single Fe monolayer in noble metals,[60] the calculated magnetic moments in these bilayers (Table IV) are significantly enhanced from that of pure Mn, Fe, Co, or Ni. We

TABLE V. The experimentally (Expt.) and theoretically (Theor.) observed spin and orbital moments for the CuAu(I)-type phases considered in the present study. Orbital moments are denoted by the subscript *o*. **A** denotes the first atom site ($3d$ element), **B** denotes the second atom. All moments are in units of μ_B atom and the total moments in μ_B/f.u.

Phase	A_o^{SO+OP}	B_o^{SO+OP}	A_o^{SO}	B_o^{SO}	A_o	B_o
CoPt (Expt.)[a]					0.28	0.24
CoPt (Expt.)[b]						0.08
CoPt (Theor.)[c]					0.12	0.07
CoPt (Theor.)[d]					0.12	0.06
CoPt [001]	0.161	0.062	0.089	0.056		
CoPt [110]	0.112	0.080	0.057	0.073		
FeNi [001]	0.080	0.047	0.051	0.035		
FeNi [110]	0.067	0.049	0.045	0.037		
FePd (Expt.)[e]					0.17	0.22
FePd (Theor.)[f]					0.19 (tot)	
FePd [001]	0.123	0.029	0.073	0.026		
FePd [110]	0.099	0.033	0.063	0.029		
FePt (Expt.)[g]					0.07	0.1
FePt (Theor.)[c]					0.08	0.05
FePt (Theor.)[d]					0.08	0.07
FePt [001]	0.110	0.048	0.067	0.042		
FePt [110]	0.096	0.063	0.061	0.055		
MnHg [001]	−0.004	0.014	−0.006	0.014		
MnHg [110]	−0.006	0.015	−0.007	0.014		
MnNi [001]	0.017	0.046	0.011	0.034		
MnNi [110]	0.014	0.038	0.009	0.029		
MnPd [001]	0.012	0.032	0.009	0.028		
MnPd [110]	0.007	0.028	0.005	0.025		
MnPt [001]	0.046	0.039	0.038	0.034		
MnPt [110]	0.037	0.030	0.029	0.026		
MnRh [001]	0.043	−0.018	0.032	−0.014		
MnRh [110]	0.057	−0.039	0.040	−0.029		
NiPt [001]	0.000	0.048	0.000	0.042		
NiPt [110]	−0.059	0.068	−0.033	0.056		

[a]See Ref. 93.
[b]See Ref. 94.
[c]See Ref. 29.
[d]See Ref. 9.
[e]See Ref. 96.
[f]See Ref. 97.
[g]See Ref. 98.

will outline the origin of the enhancement of the spin moments in Fe*X* phases and apply this to the other systems considered here. In the CuAu(I)-type structure, both Fe and *X* have only four nearest neighbors of the same type and this makes the hybridization between the same type of atoms weaker compared with that in the fcc structure. Further, the site-, spin-, and angular-momentum-projected DOS of the Fe*X* phases given in Fig. 4 indicate that the lower energy part of the Fe $3d^{\downarrow}$ states are almost empty which makes one-spin channel of the *d* electrons not participating in the covalent interaction with neighboring atoms. This weaker hybridization effect usually narrows the bandwidths[61] and enhances the exchange splitting. Furthermore, the large exchange splitting is due to considerable tetragonal distortion along with the volume expansion that produces band narrowing and a larger magnetic moment. The observation of induced magnetism on the Pd/Pt site is consistent with experimental studies in the sense that spin-resolved and spin-integrated, angle-resolved photoemission studies[62] reveal magnetic polarization of Pd and Pt at the interface with a ferromagnetic substrate. The XMCD studies show induced spin polarization in nonmagnetic metals for Co/Pt (Ref. 63) and Fe/Pd multilayers.[63–65] Also, Koide *et al.*[54] measured XMCD spectra for Fe/Pt multilayer films and found an induced moment on the Pt atoms aligned parallel to the Fe moments.

The good agreement for the orbital moment of fcc and hcp Co obtained from the present type of SO+OP calculation[35] compared with recent XMCD measurements,[66] indicates that the predicted orbital moments (Table V) are reliable. From Table V it should be noted that all Mn*X* phases possess considerable orbital moments for both magnetization directions, however, the orbital moments are small due to the fact that Mn is close to a half-filled shell system.

Furthermore, the orbital moment at the Mn site is not changed dramatically on going to other metal components. For CoPt we obtained from our SO+OP calculations an orbital moment of 0.112 and $0.161\mu_B$/atom for Co, respectively with spin quantization along [110] and [001]. The latter value agrees with the recent XMCD value[66] of $0.16 \pm 0.01\mu_B$/atom for the Co/Pt interface layer. The larger orbital moment along [001] compared with that of hcp Co ($0.148 \pm 0.005\mu_B$/atom) indicates that the reduced bandwidth and enhanced spin moment play an important role in MAE. Further, hybridization induces magnetism on the Pt atoms and their orbital moments are aligned parallel to that of Co. The considerable OMA at the Pt site in CoPt indicates that both Co and Pt contribute to PMA. As noted by Sakuma[29] for FePt and CoPt, the spin-orbit coupling of Pt is roughly ten times larger than that of a $3d$ transition metal. Hence, the considerable orbital moment of Pt is a combined effect of the hybridization with the neighboring magnetic elements and its large spin-orbit interaction (SOI) strength.

It is well known that the splitting of electron-energy states in the magnetic quantum number levels (m_l) due to SOI interaction is the origin of orbital moment. Since the size of the orbital moment is to a large degree caused by a redistribution of electron states around the Fermi level,[37] it generally scales to some degree with the value of DOS at E_F. However, in addition the crystal symmetry is important since low symmetric phases are usually found to have the largest orbital moment. To improve the understanding of the orbital moments, Fig. 5 shows the spin-projected orbital moments for FeX as a function of band filling for the moment aligned along [001] as obtained from SO+OP calculations. Owing to the partial cancellation of spin-up and spin-down contributions one finds only a very small value of the total orbital moment on the Fe and X sites (see Fig. 5). These results indicate a close correlation between values for the orbital magnetic moments and the spin-polarized electronic structure near E_F. From Table V it is seen that materials possessing large exchange splitting and SO strength usually have large orbital moments. This can be understood in the following way. A spin-degenerate calculation, even if it includes the SO interaction, will yield a zero orbital moment. Thus, a spin moment that is reduced (approaches zero) produces an orbital moment that is also reduced (approaches zero). Conversely, increased spin moments (viz., increased exchange splitting) generally produce larger orbital moments. Even though Pd and Pt are nonmagnetic in their elemental form, they possess considerable orbital moments in the phases considered here. This is due to the combined effect of large SO and induced spin moments.

From Tables V it is clear that OP usually enhances the orbital moment, and these values approach the experimental ones. The origin of the enhancement may be explained as follows. The expression for the orbital-polarization energy is obtained by a mean-field treatment[35] of the interaction $l_i l_j$ (l_i being the orbital moment of electron i). This means that at the variational step and for each $\mathbf{k}$ point an orbital with azimuthal and magnetic quantum number, (l,m_l) will be shifted by an amount Bm_lL. This shifting always enhances the orbital moment and hence the magnetic anisotropy. Further,

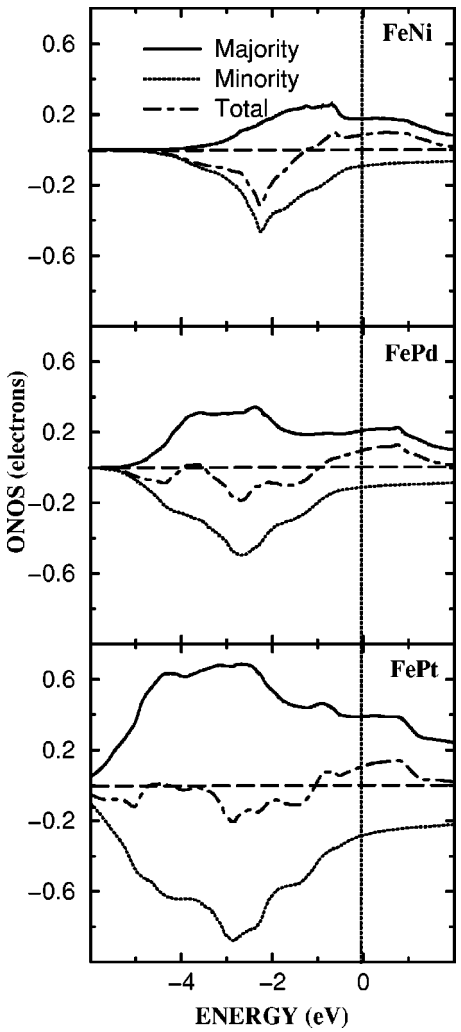

FIG. 5. Orbital-moment number of states (ONOS) or orbital moment as a function of energy as obtained from SO+OP calculation with the quantization axis along [001] for FeX.

within perturbation theory[67] the orbital angular momentum is proportional to the SO parameter ξ and for the limit of large exchange splitting a new orbital angular momentum, $L = L_o/(1 - L_o B/\xi)$, results upon including the orbital polarization, where L_o is the orbital angular momentum obtained without orbital polarization. Hence, OP represents an effective spin-orbit coupling parameter $\xi' = \xi + BL$. These features cause a large value of the orbital moment and magnetic anisotropy when OP is included in the calculations.

The orbital moment on the Pt site is larger than that of Ni and Pd in FeX phases as given in Table V. From Fig. 4 it is clear that the Pt-$5d$ DOS is much broader in the valence band (VB) than Ni $3d$ and Pd $4d$ DOS due to screening effects. Hence, the larger moment is attributed to the much higher degree of hybridization between Pt($5d$)-Fe($3d$) than Pd($4d$)-Fe($3d$) or Ni($3d$)-Fe($3d$). Apart from the hybridization effect, the large SOI of Pt also plays an important role in the enhancement of the orbital moment. Except for NiPt, MnHg, and MnRh the orbital moments of both constituents align parallel to the spin moment (see Table IV). It is interesting to note that except MnHg and NiPt, the calcu-

lated orbital moments on the $3d$-transition-metal sites are larger than those on the $4d/5d$-transition-metal sites (Table V). The reason is a strong mutual cancellation of the spin-up and spin-down contribution on the $4d/5d$ site, rather than a low value of SOI for these sites (see Fig. 5). The small value of the orbital moment in transition metals compared with the transition metal compounds considered here is a consequence of the well-known crystal-field quenching of the orbital moment together with the fact that the spin-orbit coupling parameter is relatively small. When we compare our calculated orbital moment (Table V) with those obtained from ASA calculations (see Table V), both SO and SO+OP always give smaller values of the orbital moment. For the SO+OP calculations a better quantitative agreement with experimental values is obtained than for the ASA calculations, indicating the importance of full-potential treatment. Regarding measurements of the orbital moment, the XMCD studies have so far only been carried out for a few multilayer films. We hope that our predicted spin and orbital moments for the bilayer materials given in Tables IV and V will motivate further experimental measurements.

C. MAE and tetragonal distortion

In the following section we analyze the different important contributions to MAE for the present systems. Apart from surface/interface anisotropies, strain anisotropies also induce perpendicular magnetization.[68–70] From the calculation of MAE along the Bain path on Ni by Hjortstam *et al.*[71] and on Co and Fe by James *et al.*[72] it has been shown that for cubic symmetry MAE is of the order of μeV /atom and breaking the cubic symmetry may enhance MAE by orders of magnitude. Hence, it is interesting to study the correlation between MAE and the tetragonal distortion in the CuAu(I)-type compounds. The c/a vs MAE relationship for the bilayer materials considered in the present study are shown in Fig. 6. It is seen that MnPt has a large tetragonal distortion along with large exchange interaction arising from Mn and SOI from Pt, and hence, possesses a large MAE. On the other hand, MnHg, despite a large exchange interaction (from Mn) and large SOI (from Hg d states), possesses low magnetic anisotropy due to c/a close to the value for cubic symmetry and a low hybridization between the Mn $3d$ and Hg $5d$ states. Further, Hg has filled d bands and the induced spin polarization for Hg is therefore negligible for MnHg (see Table IV). In MnAl, none of the constituents possess large SOI. Despite these features MnAl possesses a comparably large value of MAE (0.341 meV) due to the fact that c/a deviates substantially from cubic symmetry (see Table II). The above results indicate the importance of larger strain/lower symmetry in order to receive large magnetic anisotropy.

The relationship between reduced symmetry and enhanced anisotropy is most readily seen when the spin-orbit coupling can be treated in terms of perturbation theory.[67] For uniaxial symmetry the anisotropy energy is proportional to ξ^2 (instead of ξ^4 for cubic symmetry) where ξ is the spin-orbit coupling constant. When c/a changes between 1 (for bcc) and $\sqrt{2}$ (for fcc), an additional contribution to MAE

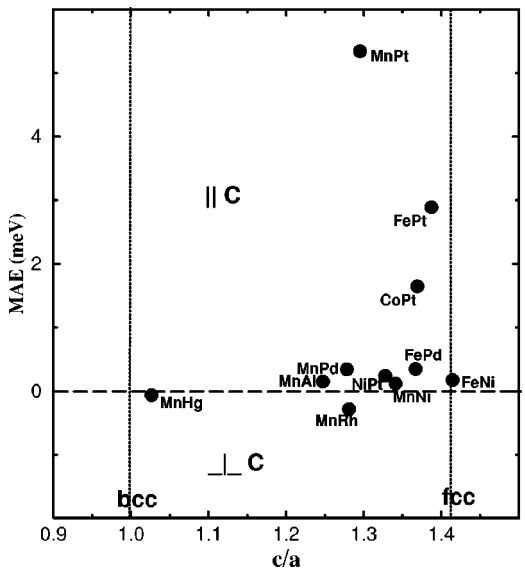

FIG. 6. Correlation between MAE and the tetragonal distortion for bilayered transition-metal phases. c/a represents the axial ratio of the simple tetragonal structure and is $\sqrt{2}$ times that of CuAu(I)-type structure.

arises from the lifting of the degeneracy of the electrons by the tetragonal crystal field. Hence, the reasons for the small MAE in cubic bulk systems is the high symmetry that only allows a fourth-order anisotropy constant. However, one should be cautious when correlating directly c/a with MAE for different phases, since MAE depends not only on symmetry changes but also on band filling, hybridization between constituents and corresponding changes of the electronic structure, etc. For the Pt phases, apart from the exchange splitting, the $(3d)$-Pt$(5d)$ hybridization plays a very important role for the anisotropy.

D. Orbital moment anisotropy and MAE

As proposed originally by van Vleck,[73] the magnetic anisotropy arises primarily from the spin-orbit interaction. Recently, angle-dependent XMCD measurements on Co_3Pt films have shown that the microscopic origin of PMA is related to $3d$ and $5d$ orbital moment anisotropies such as out-of-plane components of the orbital moments being higher than the in-plane components.[74] For uniaxial layered materials, MAE may be defined as $\Delta E = E^{\perp} - E^{\parallel}$, where $\perp$ and $\parallel$ stand for the magnetization perpendicular to and within the layers, respectively. In order to understand the first principle result, a perturbation expression for MAE was found to be very helpful.[7] Due to the large exchange splitting (about 2 eV for Mn, Fe, and Co in these phases), contributions from spin-orbit coupling (SOC) between spin-down states dominate the SOC-induced energy changes and thus we can simplify MAE from the various transition metal sites to

$$\Delta E = E^{\parallel} - E^{\perp} \approx \xi^2 \sum_{u,f} \frac{|\langle u|L_z|f\rangle|^2 - |\langle u|L_x|f\rangle|^2}{\epsilon_u - \epsilon_f}, \qquad (7)$$

where u and f stand for unoccupied and filled spin-down states, respectively. Thus, if the coupling through L_z is stronger, perpendicular magnetization prevails (positive MAE energy) and vice versa. Bruno[75] showed, using perturbation theory and assuming that the exchange splitting is larger than the bandwidth for a $3d$ element with more than half-filled d shell, that the following relationship holds between MAE and OMA:

$$\Delta E \propto -\frac{\xi}{4\mu_B}[M_0^{\perp} - M_0^{\parallel}], \tag{8}$$

where $M_0^{\perp}$ and $M_0^{\parallel}$ are the orbital moment for magnetization perpendicular and within the plane, respectively, and ξ is the spin-orbit parameter. The above relation states that for perpendicular magnetic anisotropy $M_0^{\perp}$ will be larger than $M_0^{\parallel}$, whereas for a preferred in-plane magnetization the reversed situation will occur. From the theoretical study by Hjortstam *et al.*[71] on tetragonally distorted fcc Ni, and by Trygg *et al.*[27] for bcc Fe, hcp Co and fcc Ni, it has indeed been concluded that the easy-magnetization axis coincides with the direction that has the largest orbital moment. Hence, if it is judged that OMA is easier to measure than MAE, one could simply take OMA and use Eq. (8) to estimate MAE. Equation (8) has been investigated experimentally for various Co-based magnetic multilayers using the XMCD-sum rules to determine the Co-orbital moment in the multilayers.[76–78]

The relationship between OMA and MAE does not always hold and it is of interest to investigate how well it holds for the present systems. In order to establish this correlation we have plotted MAE vs OMA ($L_{001} - L_{110}$) in Fig. 7. It is interesting to note that except FePt, all the materials that possess perpendicular anisotropy (i.e., with positive MAE in Fig. 7 and [001] being the easy axis) the abovementioned correlation holds well. There is, however, no straightforward proportionality between OMA and the corresponding anisotropy energies. This implies that the relationship between the orbital moments and magnetic anisotropy energies is much more complicated for bilayer systems than for the simple cases discussed above.[75] From the XMCD measurements of orbital moments and the magnetic anisotropy for Co/X (X = Ni, Pd, Pt) Weller *et al.*[76] concluded that these multilayers possess PMA and showed that the out-of-plane orbital moment of Co in Co/Pd and Co/Pt multilayers are larger than in-plane. Our calculated result for CoPt is consistent with these experimental results in the sense that we have found PMA and also the orbital moment of Co larger in out-of-plane than in-plane. The orbital moment of Co in CoPt is much smaller than that in YCo_5 (where Co has an orbital moment of $0.24–0.26\mu_B$),[79] which possesses strong PMA. Hence, the large PMA in CoPt must have a substantial contribution from Pt that exhibits a considerable induced orbital moment. A recent XMCD study[66] on Co/Pt multilayers is in support of this view and indicates that PMA is caused by anisotropy in orbital moments and originates from Pt 5d–Co $3d$ hybridization. A straightforward extension of Eq. (8) for bilayer systems has been derived[80]

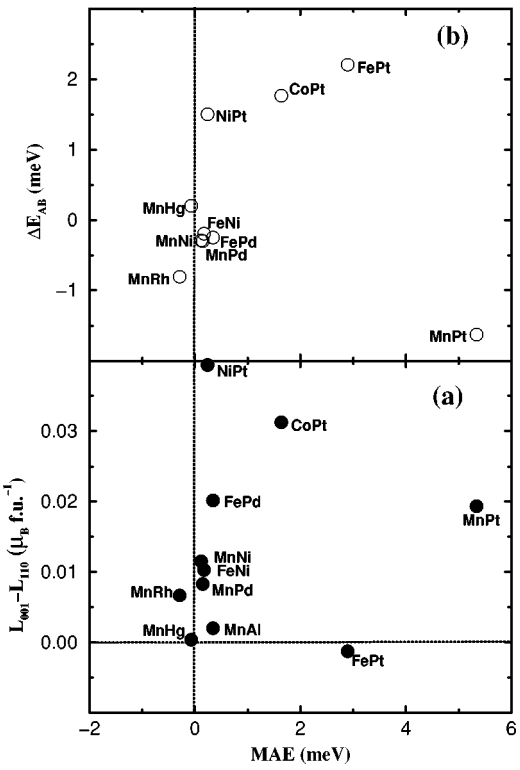

FIG. 7. (a) Anisotropy in orbital moment ($L_{001} - L_{110}$) vs MAE for bilayered materials obtained from SO+OP calculations. Positive (negative) value for the y axis means that large orbital moments are pointing along the [001] ([110]) axis. (b) The ΔE_{AB} vs MAE for bilayered materials obtained from SO+OP calculations.

$$\Delta E_{AB} = \Delta E_A + \Delta E_B = -\frac{1}{4\mu_B}[\xi_A(M^o_{001} - M^o_{110})_A] - \frac{1}{4\mu_B}[\xi_B(M^o_{001} - M^o_{110})_B] + E_B^{+-} + E_B^{-+}. \tag{9}$$

In this equation A denotes a magnetic $3d$ element, such as Fe, with large exchange splitting and B a ligand atom, such as Pt, where the exchange splitting is almost vanishing. Using the approximate data for ξ obtained from a standard free-atom calculation and the data of orbital moments given in Table V we have calculated the ΔE_{AB} using the first two terms in Eq. (9). From the calculated ΔE_{AB} as a function of MAE obtained from the SO+OP calculations shown in Fig. 7(b) we found that except MnPt all the other compounds fall closely to a straight line with slope 1:1. We note from this equation that the contribution from the magnetic atoms, e.g., Fe, is similar to the expression for the pure elements. However, the nonmagnetic ''B atoms'' contribute to the MAE both with a term that involves the anisotropy of the orbital moment but also with two other terms E_B^{+-} and E_B^{-+}. These represent couplings between states that are not diagonal in spin, i.e., they couple spin-up $(+)$ and a spin-down $(-)$ states. For atoms with large exchange splitting this coupling vanishes. Hence, if the contribution from the nonmagnetic atoms is large, as would be the case for heavy elements such

as Pt and Hg, the linearity between orbital moment and MAE should not hold, something that Fig. 7(a) shows.

For MnRh and MnHg the calculations predict in-plane anisotropy, but with large orbital moments pointing along [001] rather than along [110]. This is against what may be expected from Eq. (8). The reason for the violation is that although the orbital moment is large along [110] (easy axis) for Mn and Rh/Hg, the orbital moments are of opposite sign. Hence, the net orbital moment becomes larger for the hard [001] in MnHg and MnRh (Table V). If one believes that the orbital-moment anisotropy of both constituents in the bilayer materials contributes to MAE, one can expect in-plane anisotropy in FePt since a large orbital moment is pointing along [110]. From Table V it should be noted that for FePt the orbital moment originating from Fe is larger for [001] than for [110], indicating that if one considers OMA to arise from Fe alone, then the above-mentioned correlation [Eq. (8)] is obeyed. Hence, we conclude that one should be cautious when applying Eq. (8) for multicomponent systems. Owing to the induced moment on Pt, the orbital moment is larger for [110] than [001], which makes the total OMA negative in FePt (Fig. 7). This demonstrates that the correlation between total OMA and MAE may not hold well for multicomponent systems where some of the constituents posses a large induced moment originating from the neighboring magnetic atoms. On the other hand, from Fig. 7(b) it is clear that there is a linear relation between ΔE_{AB} and MAE. This indicates that the MAE originating from the combined effect of anisotropy in the orbital moment and SOI. As discussed by Solovyev *et al.*,[30] the anisotropy in FePt is mainly originating from Pt in FePt. So, large MAE in FePt is the combined effect of the large SOI and the anisotropy in the orbital moment in the Pt site in FePt. The large deviation of MnPt from the linear relation in Fig. 7(b) indicate that apart from OMA the spin-flip contributions play an important role in deciding MAE in multicomponent systems.

E. MAE and band filling

MAE depends[26] quite strongly on the unit-cell dimensions of the structural arrangement and the location of Fermi energy on the DOS curve. The sensitivity of MAE upon band filling can be used in practice to modify the MAE by chemical substitution. Hence, MAE calculations as a function of band filling are useful. Figure 8 shows the orbital-moment density of states for the [001] direction obtained from the relation $m_{\ell,\sigma}D^{\hat{n}}_{m_\ell\tau}$, where $D^{\hat{n}}_{m_\ell\tau}$ is the density of states for orbital quantum number m_ℓ for the atom τ, spin σ, and magnetization direction $\hat{n}$. From this illustration it can be seen that ODOS for the Fe site changes considerably when going from FeNi to FePt, even though the Fe spin moment does not change significantly (Table IV). Especially the amplitude of the Fe ODOS increases on going from FeNi to FePt. Further, the Fe ODOS in FeNi has same sign as that of Ni, but on the other hand, it has opposite sign to that of Pt in FePt in most of the energy range. In order to obtain a more clear picture, the orbital-moment number of states for the

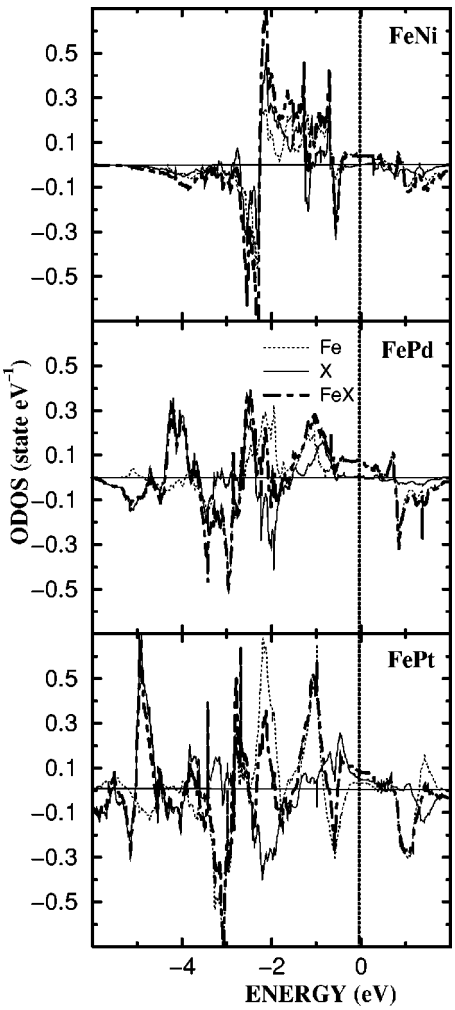

FIG. 8. Orbital-moment density of states (ODOS) as obtained from SO+OP calculations for FeX (X=Ni, Pd, Pt) for the spin-quantization direction along [001].

FeX phases in the [001] magnetization direction (Fig. 5) are calculated by integration of the ODOS curve using the relation

$$M^{\hat{n}}_{\sigma}(\epsilon)=\int_{-\infty}^{\epsilon}\sum_{m_\ell\sigma} m_\ell D^{\hat{n}}_{m_\ell\sigma}(\epsilon)d\epsilon. \tag{10}$$

The ONOS value at E_F in Fig. 5 corresponds to the orbital moments given in Table V. It should be noted that the ONOS values increase on going from FeNi to FePt due to increased spin-orbit interaction from the X atom. For cubic symmetry the orbitals group into degenerate e_g ($d_{x^2-y^2}$ and $d_{3z^2-r^2}$) and t_{2g} (d_{xy},d_{yz},d_{zx}) sets. The tetragonal distortion further lifts the above degeneracy of the d states and this leads to enhancement of the orbital moment. The opposite sign of ONOS in Fig. 5 for majority- and minority-spin states are understood as follows. When the spin-orbit coupling is introduced in the band Hamiltonian, there will be matrix elements of the type L_zS_z (and $L_+S_-+L_-S_+$). Hence, the spin-up electron states with positive (negative) quantum numbers m_l will be pushed up (down). Exactly the opposite is found for spin-down electrons, viz., the contribution to the total orbital

moment for the spin-up (-down) electrons is negative (positive). Due to exchange splitting the states for one spin direction will be preferentially occupied. Hence, the cancellation between different spins will be partially broken and an orbital magnetization obeying Hund's third rule is formed. Thus, the size of the orbital moment depends on the spin splitting. Larger spin polarization is important for the unquenching of orbital moments at $3d$ sites. From Fig. 5 it is clear that the orbital moment is formed mainly by spin-down states and is renormalized by a smaller and opposite contribution from nearly occupied spin-up states in all the cases.

It has been shown that a rigid-band approximation works well to describe trends in MAE and OMA for alloys involving Fe, Co, and Ni.[80] Moreover, earlier studies[9] indicate that there is a simple correspondence between the anisotropy in orbital moment and MAE for a wide range of band fillings in Co-based multilayers. Hence, it is interesting to study the role of band filling on the anisotropy of the orbital moment since this will give ideas about small perturbation in MAE caused by impurities, surfaces, interfaces, and hole/electron doping in multilayer films. It is difficult to envisage the anisotropy from ONOS in Fig. 5. We have therefore calculated the difference in the ONOS (ΔONOS) from the relation $M_\sigma^{[110]}(\epsilon)-M_\sigma^{[001]}(\epsilon)$ for the FeX phases as a function of band filling obtained from SO and SO+OP calculations for majority-spin, minority-spin, and total electrons. Due to the space limitation we have given the ΔONOS obtained from SO+OP calculation alone in Fig. 9. The value of ΔONOS at the Fermi energy is nothing but the difference in orbital moment and is proportional to MAE according to Eq. (8). From our studies we found that when OP correction is included, ΔONOS(E) does not change significantly for FeNi, whereas larger changes are found for FePt. The reason is that the OP correction scale with ξ according to Eq. (1) and hence the influence of OP will be larger for materials with large ξ. Further, the extended nature of Pd $4d$ and Pt $5d$ states over Ni $3d$ states, the strong hybridization of Fe $3d$ and Pd $4d$/Pt $5d$ bands, and the large spin-orbit coupling of Pd/Pt cause an increase in OMA and PMA for FePd and FePt.

The band-filling dependence of OMA is quantitatively different for the FeX phases although isostructural and isoelectronic (with respect to valence electrons), FePd and FePt have larger OMA than FeNi. Hence, it is difficult to predict MAE from the simple, rigid band-filling picture, i.e., from the ΔONOS(E) curve for related systems. From Fig. 9 it is clear that MAE of multilayers is not solely due to the reduced symmetry of the atoms at the interfaces, as in Néel's model of surface anisotropy, but depends also on the interface electronic structure. Our calculation shows that the OP correction influences the ΔONOS(E) curve in the whole energy range under consideration. It is evident from the figure that the large anisotropy in FePd and FePt at E_F originates from the majority-spin electrons. On the other hand in FeNi the minority-spin electrons are mainly contributing to the magnetic anisotropy. Although we are unable to quantitatively correlate OMA with MAE, Fig. 9 shows clearly that OMA increases systematically on going from FeNi to FePt. These factors added up to the increase in calculated MAE from 0.172 meV for FeNi to 2.891 meV for FePt (Table III).

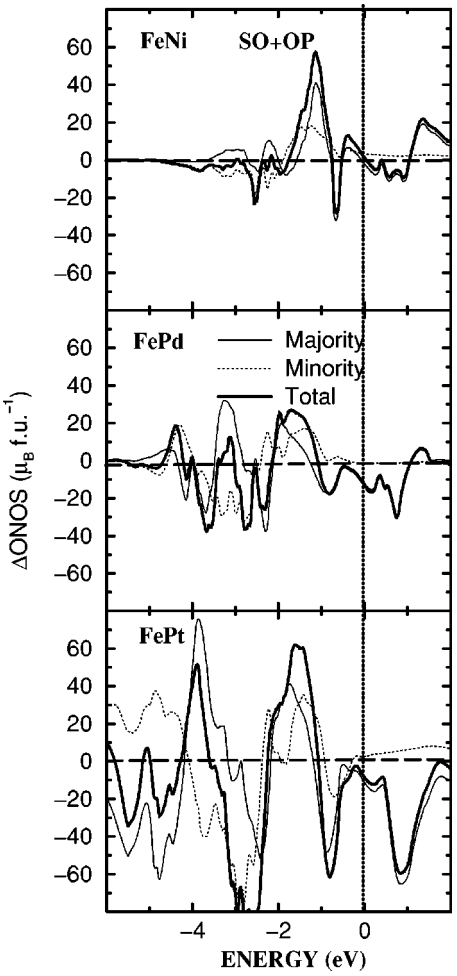

FIG. 9. Anisotropy in orbital-moment number of states ΔONOS (difference in orbital moment between [001] and [110]) as a function of energy for FeX (X=Ni, Pd, Pt) according to SO+OP calculation.

The derived values from the SO+OP calculations are almost twice those obtained from SO calculations, however, the shape of the OMA curves obtained from SO and SO+OP calculations are almost the same. For the latter reason, one expects qualitatively the same MAE dependence on band filling in both cases. Further, if rigid band-filling considerations work for small hole-doping one can from Fig. 9 expect that MAE will decrease for both FePd and FePt, but increase for FeNi. On the other hand, since OMA is increasing on electron doping for the three phases, this will favor an increase in MAE. From Fig. 9 it is seen that the orbital-moment anisotropy in the majority and minority spins is of opposite sign in certain energy ranges and of the same sign in others. As mentioned earlier, the orbital moments for the majority- and the minority-spin states are always of opposite sign over the whole energy range (Fig. 5). The important aspect of Fig. 9 is that the contribution from minority-spin state at the Fermi level is almost negligible in the three FeX phases. This is due to the almost completely filled nature of the majority-spin band. This may be the possible reason for large MAE in these systems. Since in most of the energy range the majority- and minority-spin states are of opposite

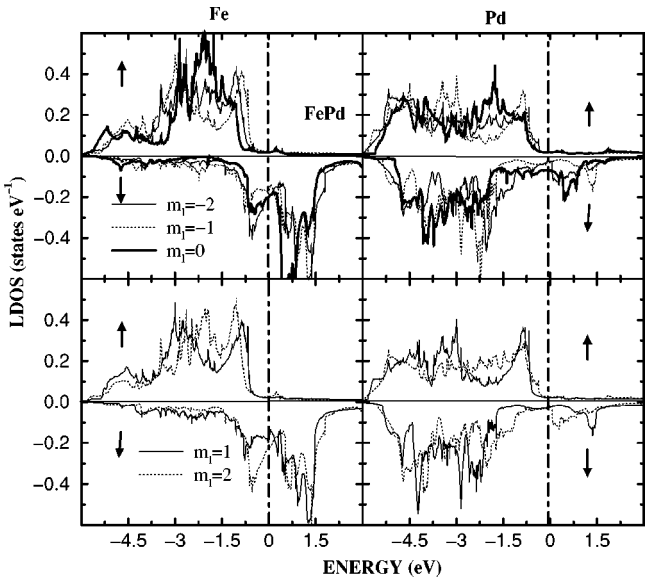

FIG. 10. Magnetic angular momentum (m_l)-projected density of states (LDOS) for -2, -1, and 0 orbitals for FePd phase. The left panel represent LDOS for Fe $3d$ electrons, the right represents that for the $4d$ electrons of Pd.

sign in ΔONOS, the total ΔONOS will be cancelled in most of the energy range. However, the negligible contribution to ΔONOS of the minority-spin channel near E_F brings the total orbital-moment anisotropy to a considerable value.

The influence of spin-orbit coupling and orbital polarization on the magnetic anisotropy is expected to be maximal in the special situation when degenerate energy bands with $m_l = \pm 2$ character occur in the vicinity of E_F. The states with $m_l = \pm 2$ character ($d_{x^2-y^2}$ and d_{xy}) have more dispersion than the states with $m_l = \pm 1$ character (d_{yz} and d_{xz}) as a consequence of their spatial form and a resulting greater overlap between orbitals on neighboring atoms is expected. The spin-orbit splitting $\pm m_l \xi_d / 2$ is large for states with the greater dispersion. From Fig. 10 it is clear that VB near E_F (i.e., -0.5 eV to E_F) is mainly dominated by $m_l = \pm 2$ character. Hence, we believe that the large magnetic anisotropy in the FeX phases is mainly originating from states with $m_l = \pm 2$ character. This is consistent with the conclusion of Daalderop *et al.*[81] for YCo_5, which is the ferromagnet with the largest MAE among transition-metal phases. Daalderop *et al.*[28] put forward two conditions for obtaining large PMA:(i) The presence of an interface between ultrathin close-packed layers and (ii) the total number of valence electrons should be such that E_F is positioned into bands with $m_l = \pm 2$ character. Wang, Wu, and Freeman[82] showed that strong, perpendicular magnetic anisotropy in Co-Pd arises from the hybridization between the out-of-plane Co bonding states and the interface Pd atoms. Daalderop *et al.*[83] also showed that the perpendicular anisotropy in a Co/Pd_2 multilayer film is caused by the location of E_F much closer to states that have mainly Co $d_{x^2-y^2}$ and d_{xy} character than in a free-standing monolayer that possesses in-plane anisotropy. Wang *et al.*[84] showed that at the Co-Cu interface, the perpendicular magnetocrystalline anisotropy contribution has been drastically decreased in magnitude, in agreement with experiment, because the bonding xz (yz) Co states are directed out of plane, and thus interact strongly with the interface Cu states. Kyuno *et al.*[85] found from electronic-structure studies on X/Co (X is a nonmagnetic metal) metallic multilayers, that the strength of the hybridization of electronic states at the interface determines the relative position of the Fermi energy in the local DOS for $|m_l| = 2$ character of Co-d electrons in minority spin. They showed further that if LDOS of $|m_l| = 2$ character is large at E_F, the system should show perpendicular anisotropy. The orbital moment in transition-metal phases originates from polarization of d electrons in m_l states due to SO and OP. Hence, it is interesting to analyze m_l projected DOS (LDOS) in detail. The s- and p-like electrons contribute negligibly to the spin density and we therefore concentrate on the contributions from the d electrons. From Fig. 10 it can be seen that the $m_l = \pm 2$ (i.e., d_{xy} and $d_{x^2-y^2}$) contributions are large at E_F for all three phases. One important observation from the LDOS curves is that for Fe the d_{xz} and d_{yz} contributions are small at E_F compared with the d_{xy}, $d_{x^2-y^2}$, and $d_{z^2-r^2}$ contributions. Also for the Pd atoms, the DOS at E_F has large contributions from the $d_{z^2-r^2}$ orbital which indicate the importance of $Fe^{\downarrow} d_{z^2-r^2} - Pd^{\downarrow} d_{z^2-r^2}$ covalent hybridization for the interface contribution to MAE. It should also be noted that although Pd is nonmagnetic, it has substantial exchange splitting due to the induced moment originating from the neighboring Fe in the FeX phases. Further, our calculations show that due to the enhancement in SOI on going from Ni to Pt, the splittings in the m_l levels or Pd/Pt $4d/5d$ levels are larger than for Ni $3d$. In all three FeX phases the minority-spin state have large LDOS with $|m_l| =$ two-character at E_F (Fig. 10) and hence show perpendicular anisotropy.[28,83,85]

F. MAE and exchange/spin-orbit interaction

Both PMA and orbital magnetic moments in solids, have common origins related to the spin-orbit interaction and exchange splitting. In order to understand the role of exchange splitting on MAE of bilayer materials, MAE vs magnetic moment for MPt (M=Mn,Fe,Co,Ni) is plotted in Fig. 11. When going from Mn to Ni in the Periodic Table, the strength of the spin-orbit coupling will not change significantly. Also, the other constituent Pt will have very similar SO strengths for all these phases. So the change in MAE when going from MnPt to NiPt is mainly due to the changes in the exchange splitting. Hence, from Fig. 11 we observe that a larger exchange splitting results in a larger MAE. Since MAE is a result of SO coupling in combination with spin polarization, the results in Fig. 11 and 12 are not too surprising. However, it is not entirely obvious that there should be a rather smooth relationship between MAE and exchange splitting, as Fig. 11 shows. Concerning the FeX and MnX phases, the SO strength will increases from X =Ni to Pt, and hence one can expect an increasing trend for the orbital moment. However, the orbital moment for these phases from SO+OP calculations (see Table IV) indicates that there is no systematic changes in the orbital moment of the X atoms when going from Ni to Pt. This can be explained

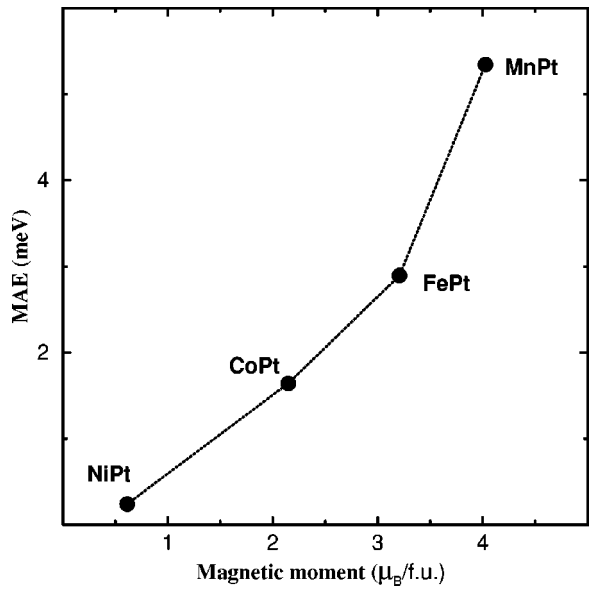

FIG. 11. Variation in MAE as a function of magnetic moment for MPt (M=Mn, Fe, Co, Ni) as obtained from SO+OP calculations.

as follows. It is well known that the orbital moment is originating from the coupling of the spin with the lattice of the system. Our calculated induced spin moment of X atoms for FeX and MnX in Table IV show a systematic decrease when going from Ni to Pt due to broadening of the d band. Hence, the orbital moment for the X atom depends on the competition between a decrease in the induced spin moment (which will decrease m_{orb} on going from Ni to Pt) and an increase in the SO strength (which will increase m_{orb} on going from Ni to Pt).

The spin-orbit coupling, responsible for the magnetocrystalline anisotropy and the orbital moment of ferromagnets, has been discussed by various authors[75,86,87] who showed that it can be approximated by a one-electron term ξls, were ξ, the spin-orbit constant, is of the order of 0.05–0.10 eV for Fe, Co, and Ni. As shown by Daalderop *et al.*,[83] the magnetic anisotropy can be related to the spin-orbit-interaction-induced splitting and shifting of electronic states that depend on the magnetization direction. In order to illustrate the role of the spin-orbit coupling strength of the coordinating atom on MAE for these phases, MAE for MnX and FeX (X =Ni,Pd,Pt) as a function of ligand-atom change is shown in Fig. 12. It is clear that the spin-orbit coupling of the ligand atom strongly influences MAE. A similar observation has been made for multilayer systems.[8] Because of the weaker hybridization between atoms of the same type within the plane, the $d_{x^2-y^2}$ and d_{xy} components of LDOS are larger than the $d_{z^2-r^2}$, d_{yz}, and d_{xz} components. Hence, the $3d$ atoms induce a magnetic moment on the coordinating atoms via strong covalent hybridization. As a result one observes a larger MAE when the spin-orbit interaction of the coordinating atom is larger.

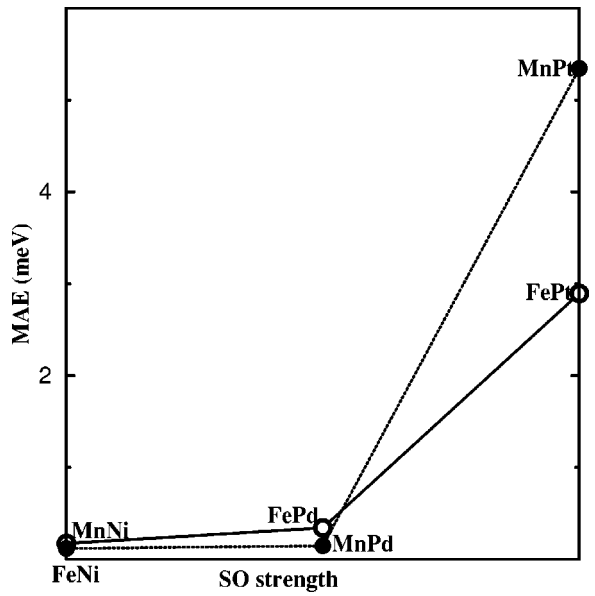

FIG. 12. Change in MAE upon variation of the spin-orbit interaction strength of coordinating atoms for FeX and MnX (X =Ni, Pd, Pt).

VI. SUMMARY

We have calculated the magnetic anisotropies and the spin and orbital moments for MnX, FeX (X=Ni,Pd,Pt), CoPt, NiPt, MnHg, and MnRh from first principles, using full-potential LSDA and LSDA+OP band-structure theory. Pronounced anisotropies in the orbital moments are obtained, in contrast to the spin moments. We have demonstrated that the accurate full-potential calculations normally reproduce the correct easy axis, and even the size of MAE is close to the experimental values when OP corrections are included. The large MAE in the bilayer materials considered here originate from the combined effects of a tetragonal structural distortion, the exchange splitting, and the spin-orbit splitting of (at least) one of the constituents. One important conclusion of the present study is that the often-quoted correlation between OMA and MAE for elements does not necessarily hold for binary phases. This has been shown from our studies on FePt, where the easy axis of magnetization is pointing along [001], on the other hand large total orbital moment is directed along the the hard axis [110]. The reason for this behavior is that the magnetic anisotropy is mainly originating from the Fe atoms, whereas the orbital-moment anisotropy is dominantly influenced by the induced moment for Pt. In most of these bilayer systems PMA results from the large anisotropy in the electronic structure caused by hybridization at the interface and from SOI, which overcomes the in-plane anisotropy provided by the magnetic dipolar interaction. The large anisotropy in MPt (M=Mn, Fe, Co, Ni) phases is shown to be due to the hybridization of the Pt $5d$ and transition-metal $3d$ states, along with a large value for the Pt $5d$ spin-orbit interaction. Our studies show that the effect of the coordinating atoms can be much larger than the effect of reduced symmetry at an interface. Finally, we note that there will be an extremely large value of MAE for MnPt provided that this material could be stabilized in a ferromagnetic condition.

ACKNOWLEDGMENTS

P.R. is thankful for the financial support from the Research Council of Norway. Part of these calculations were carried out on the Norwegian supercomputer facilities. O.E., B.J., and L.N. wish to thank the Swedish Natural Science Foundations (NFR and TFR) for support. The support from the European training and mobility program (TMR) is also acknowledged. P.R. wishes to thank Dr. Olof Hjortstam, Professor Claudia Ambrosch-Draxl, Dr. Peter Oppeneer, and Professor Mike Brooks for useful discussions and Dr. John Wills for supplying the FP-LMTO code used in this study.

*Electronic address: ravindran.ponniah@kjemi.uio.no

[1] J. C. Lodder, MRS Bull. **20**, 59 (1995); J. L. Simonds, Phys. Today **48** (4), 26 (1995).
[2] E. S. Murdock, R. F. Simmons, and R. Davidson, IEEE Trans. Magn. **MAG-28**, 3078 (1992).
[3] H. Brooks, Phys. Rev. **58**, 909 (1940).
[4] M. B.Stearns, in *3d, 4d, and 5d Elements, Alloys and Compounds*, edited by H. P. J. Wijn, Landolt-Börnstein, New Series, Group III, Vol. 19, Pt. a (Springer, Berlin, 1986), p. 34.
[5] D. Weller, G. R. Harp, R. F. C. Farrow, A. Cebollada, and J. Sticht, Phys. Rev. Lett. **72**, 2097 (1994).
[6] T. Suzuki, D. Weller, C.-A. Chang, R. Savoy, T. Huang, B. A. Gurney, and V. Speiosu, Appl. Phys. Lett. **64**, 2736 (1994).
[7] D. S. Wang, R. Wu, and A. J. Freeman, Phys. Rev. B **47**, 14 932 (1993).
[8] G. H. O. Daalderop, P. J. Kelly, and M. F. H. Schuurmans, Phys. Rev. B **42**, 7270 (1990).
[9] G. H. O. Daalderop, P. J. Kelly, and M. F. H. Schuurmans, Phys. Rev. B **44**, 12 054 (1991).
[10] C. Chappert and P. Bruno, J. Appl. Phys. **64**, 5736 (1988).
[11] L. Néel, J. Phys. Radium **15**, 225 (1954).
[12] L. Zhong, M. Kim, X. Wang, and A. J. Freeman, Phys. Rev. B **53**, 9770 (1996).
[13] X. Wang, R. Wu, D. Wang, and A. J. Freeman, Phys. Rev. B **54**, 61 (1996).
[14] U. Gradmann and J. Müller, Phys. Status Solidi **27**, 313 (1968).
[15] P. F. Carcia, A. D. Meinholdt, and A. Suna, Appl. Phys. Lett. **47**, 178 (1985).
[16] F. J. A. den Broeder, D. Kuiper, H. C. Donkersloot, and W. Hoving, Appl. Phys. A: Solids Surf. **49**, 507 (1989); C. H. Lee, R. F. C. Farro, C. L. Lin, and E. E. Marinero, Phys. Rev. B **42**, 11 384 (1990).
[17] F. J. A. den Broeder, D. Kuiper, A. P. van de Mosselaer, and W. Hoving, Phys. Rev. Lett. **60**, 2769 (1988).
[18] D. G. Stinson and S.-C. Shin, J. Appl. Phys. **67**, 4459 (1990).
[19] B. Heinrich, J. F. Cochran, M. Kowakwski, J. Kisrschner, Z. Celinski, A. S. Arrott, and K. Myrtte, Phys. Rev. B **44**, 9348 (1991).
[20] M. Sakurai, Phys. Rev. B **50**, 3761 (1994).
[21] M. T. Johnson, P. J. H. Bloemen, F. J. A. den Broeder, and J. J. de Vries, Rep. Prog. Phys. **59**, 1409 (1996).
[22] P. F.Carcia, in *Proceedings of the International Symposium on Physics of Magnetism Magnetic Materials, Sendai, Japan*, edited by M. Takahashi, S. Maekawa, Y. Gondo, and H. Noso (World Scientific, Singapore, 1987), p. 240.
[23] T. Klemmer, D. Hoydick, H. Okumura, B. Zhang, and W. A. Soffa, Scr. Metall. Mater. **33**, 1793 (1995).
[24] K. R. Coffey, M. A. Parker, and J. K. Howard, IEEE Trans. Magn. **31**, 2737 (1995).
[25] S. Hashimoto, H. Matsuda, and Y. Ochiai, IEEE Trans. Magn. Jpn. **7**, 362 (1992).
[26] G. H. O. Daalderop, P. Kelly, and M. Schurmans, Phys. Rev. B **41**, 11 919 (1990).
[27] J. Trygg, B. Johansson, O. Eriksson, and J. M. Wills, Phys. Rev. Lett. **75**, 2871 (1995).
[28] G. H. O. Daalderop, P. J. Kelly, and F. J. A. den Broeder, Phys. Rev. Lett. **68**, 682 (1992).
[29] A. Sakuma, J. Phys. Soc. Jpn. **63**, 3053 (1994).
[30] I. V. Solovyev, P. H. Dederichs, and I. Mertig, Phys. Rev. B **52**, 13 419 (1995).
[31] P. M. Oppeneer, J. Magn. Magn. Mater. **188**, 275 (1998).
[32] B. T. Thole, P. Casra, F. Sette, and G. van der Laan, Phys. Rev. Lett. **68**, 1943 (1992); P. Carra, B. T. Thole, M. Altarelli, and X.-D. Wang, *ibid.* **70**, 694 (1993); R. Wu, D. Wang, and A. J. Freeman, J. Magn. Magn. Mater. **132**, 103 (1994).
[33] Y. Wu, J. Stöhr, B. D. Hermsmeier, M. G. Sarmant, and D. Weller, Phys. Rev. Lett. **69**, 2307 (1992); T. Böske, W. Clemens, C. Carbone, and W. Eberhardt, Phys. Rev. B **49**, 4003 (1994); Y. U. Idzerda, C. J. Guttierrez, L. H. Tjeng, H.-J. Lin, G. Meigs, and C. T. Chen, J. Magn. Magn. Mater. **127**, 109 (1993); G. van der Laan, M. A. Hoyland, A. Surman, G. F. J. Flipse, and B. T. Thole, Phys. Rev. Lett. **69**, 3827 (1992).
[34] M. S. S. Brooks, Physica B **130**, 6 (1985); O. Eriksson, M. S. S. Brooks, and B. Johansson, Phys. Rev. B **41**, 9087 (1990).
[35] O. Eriksson, M. S. S. Brooks, and B. Johansson, Phys. Rev. B **41**, 7311 (1990).
[36] O. Eriksson, B. Johansson, R. C. Albers, A. M. Boring, and M. S. S. Brooks, Phys. Rev. B **42**, 2707 (1990).
[37] P. Söderlind, O. Eriksson, R. C. Albers, A. M. Boring, and B. Johansson, Phys. Rev. B **45**, 12 911 (1992).
[38] J. M. Wills (unpublished); J. M. Wills and B. R. Cooper, Phys. Rev. B **36**, 3809 (1987); D. L. Price and B. R. Cooper, *ibid.* **39**, 4945 (1989).
[39] O. Hjortstam, L. Nordström, B. Johansson, J. M. Wills, and O. Eriksson (unpublished).
[40] H. J. F. Jansen, J. Appl. Phys. **67**, 4555 (1990).
[41] O. Eriksson, M. S. S. Brooks, and B. Johansson, Phys. Rev. B **41**, 9087 (1990).
[42] G. Racah, Phys. Rev. **61**, 186 (1942).
[43] C. K. Jörgensen, *Orbitals in Atoms and Molecules* (Academic Press, London, 1962), Chap. 2, p. 19.
[44] C. T. Chen, Y. U. Idzerda, J. J. Lin, N. V. Smith, G. Meigs, E. Chaban, G. H. Ho, E. Pellegrin, and F. Sette, Phys. Rev. Lett. **75**, 152 (1995).
[45] M. S. S. Brooks and P. J. Kelly, Phys. Rev. Lett. **51**, 1708 (1983).
[46] U. Gradmann, J. Korecki, and G. Waller, Appl. Phys. A: Solids Surf. **A39**, 1 (1986).
[47] M. B. Stearns, in 3*d*, 4*d*, 5*d Elements, Alloys and Compounds*,

edited by H. P. J. Wijn, Landolt-Börnstein, New Series, Group III, Vol. 19 (Springer-Verlag, Berlin, 1986).
[48] W. L. O'Brien and B. P. Tonner, J. Appl. Phys. **76**, 6468 (1994).
[49] J. C. Suits, IBM J. Res. Dev. **19**, 422 (1975).
[50] Y.-S. Kim and S.-C. Shin, Phys. Rev. B **59**, R6597 (1999); S.-C. Shin, G. Srinivas, Y.-S. Kim, and M.-G. Kim, Appl. Phys. Lett. **73**, 393 (1998).
[51] R. Krishnan, H. Lasson, S. Prasad, M. Pote, and M. Tessier, J. Appl. Phys. **73**, 6433 (1993).
[52] E. Colombo, O. Donzelli, G. B. Fratucello, and F. Ronconi, J. Magn. Magn. Mater. **93**, 597 (1991).
[53] S. Mitani, K. Takanashi, M. Sano, H. Fujimori, A. Osawa, and H. Nakajima, J. Magn. Magn. Mater. **148**, 163 (1995).
[54] T. Koide, T. Shidara, K. Yamaguchi, A. Fujimori, H. Fukutani, N. Nakajima, T. Sugimoto, T. Katayama, and Y. Suzuki, Phys. Rev. B **53**, 8219 (1996).
[55] J.-P. Kuang, M. Kontani, M. Matsui, and K. Adachi, Physica B **149**, 209 (1988).
[56] A. Kootte, C. Haas, and R. A. de Groot, J. Phys.: Condens. Matter **3**, 1133 (1991).
[57] D. J. Gillespie and A. I. Schindler, in *Magnetism and Magnetic Materials—1971*, edited by C. D. Graham and J. J. Rhyne , AIP Conf. Proc. No. 5 (AIP, New York, 1972), p. 461.
[58] R. Kuentzler, in *Physics of Transition Metals*, edited by P. Rhodes, IOP, Conf. Proc. No. 55 (Institute of Physics, London, 1980), p. 397.
[59] P. E. Brommer and J. J. M. Franse, Physica B **149**, 221 (1988).
[60] G. Y. Guo, W. M. Temmerman, and H. Ebert, J. Phys.: Condens. Matter **3**, 8205 (1991).
[61] O. K. Andersen, H. L. Skriver, H. Nohl, and B. Johansson, Pure Appl. Chem. **52**, 93 (1979).
[62] W. Weber, D. Hartmann, D. A. Wesner, and G. Güntherodt, J. Magn. Magn. Mater. **104-107**, 1791 (1992).
[63] G. Schütz, R. Wienke, W. Wilhelm, W. B. Zeper, H. Ebert, and K. Sport, J. Appl. Phys. **67**, 4456 (1990).
[64] M. Li, X. D. Ma, C. B. Peng, J. G. Zhao, L. M. Mei, Y. S. Gu, W. P. Chai, Z. H. Mai, B. G. Shen, Y. H. Liu, and D. S. Dai, Phys. Rev. B **50**, 10 323 (1994).
[65] J. Vogel, A. Fontaine, V. Cros, F. Petroff, J. P. Keppler, G. Krill, A. Rogalev, and J. Gordon, Phys. Rev. B **55**, 3663 (1997).
[66] N. Nakajima, T. Koide, T. Shidara, H. Miyauchi, H. Fukutani, A. Fujimori, K. Ito, T. Katayama, M. Nyvlt, and Y. Suzuki, Phys. Rev. Lett. **81**, 5229 (1998).
[67] J. Friedel, in *The Physics of Metals*, edited by J. M. Ziman (Cambridge Univ. Press, Cambridge, 1969).
[68] U. Gradmann, Ann. Phys. (Leipzig) **17**, 91 (1966).
[69] R. Jungblut, M. T. Johnson, J. A. de Stegge, A. Reinders, and F. J. A. den Broeder, J. Appl. Phys. **75**, 6424 (1994).
[70] B. Schulz and K. Baberschke, Phys. Rev. B **50**, 13 467 (1994).
[71] O. Hjortstam, K. Baberschke, J. M. Wills, B. Johansson, and O. Eriksson, Phys. Rev. B **55**, 15 026 (1997).
[72] P. James, O. Hjortstam, O. Eriksson, B. Johansson, and L.Nordström (unpublished).
[73] J. H. van Vleck, Phys. Rev. **52**, 1178 (1937).
[74] W. Grange, J. P. Kappler, M. Maret, J. Vogel, A. Fontaine, F. Petroff, G. Krill, A. Rogalev, J. Goulon, M. Finazzi, and N. Brooks, J. Appl. Phys. **83**, 6617 (1998); Phys. Rev. B **58**, 6298 (1998).
[75] P. Bruno, Phys. Rev. B **39**, 865 (1989).
[76] D. Weller, Y. Wu, J. Stöhr, M. G. Samant, B. D. Hermsmeier, and C. Chappert, Phys. Rev. B **49**, 12 888 (1994).
[77] D. Weller, in *Spin-Orbit Influenced Spectroscopies of Magnetic Solids*, edited by H. Ebert and G.Schütz (Springer, Berlin, 1996), p. 1.
[78] D. Weller, J. Stöhr, A. Carl, M. G. Samant, C. Chappert, R. Mégy, P. Beauvillain, P. Veillet, and G. A. Held, Phys. Rev. Lett. **75**, 3752 (1995).
[79] H. Heidemann, D. Richter, and K. H. J. Bushow, Z. Phys. B **22**, 367 (1975).
[80] P. James, L. Nordstrüm, B. Johansson, and O.Eriksson (unpublished).
[81] G. H. O. Daalderop, P. J. Kelly, and M. F. H. Schuurmans, Phys. Rev. B **53**, 14 415 (1996).
[82] D. S. Wang, R. Wu, and A. J. Freeman, Phys. Rev. B **48**, 15 886 (1993).
[83] G. H. O. Daalderop, P. J. Kelly, and M. F. H. Schuurmans, Phys. Rev. B **50**, 9989 (1994).
[84] D. S. Wang, R. Wu, and A. J. Freeman, J. Magn. Magn. Mater. **129**, 237 (1994).
[85] K. Kyuno, J.-G. Ha, R. Yamamoto, and S. Asano, J. Appl. Phys. **79**, 7084 (1996).
[86] G. C. Fletcher, Proc. Phys. Soc., London, Sect. A **67**, 505 (1954).
[87] J. Friedel, P. Lenglart, and G. Leman, J. Phys. Chem. Solids **25**, 781 (1964).
[88] V. V. Maykov, A. Ye Yermakov, G. V. Ivanov, V. I. Khrabrov, and L. M. Magat, Phys. Met. Metallogr. **67**, 76 (1989).
[89] P. Brissoneau, A. Blanhard, and H. Bartolin, IEEE Trans. Magn. **MAG-2**, 479 (1966).
[90] V. G. Pyn'ko, L. V. Zhivayeva, N. A. Ekonomov, A. S. Komalov, N. N. Yevtikhiyev, and A. R. Krebs, Phys. Met. Metallogr. **45**, 179 (1979).
[91] P. Kamp, A. Marty, B. Gilles, R. Hoffmann, S. Marchesini, and M. Belokhovsky, C. Boeglin, H. A. Dürr, S. S. Dhesi, G. Van der Laan, and A. Rogalev, Phys. Rev. B **59**, 1105 (1999).
[92] L. M. Magat, A. S. Yermolenko, and G. V. Ivanova, Fiz. Met. Metalloved. **26**, 511 (1968).
[93] B. van Laar, J. Phys. (Paris) **25**, 600 (1964).
[94] H. Maruyama, A. Urata, N. Kawamura, H. Yamazaki, E. K. Hill, D. Raoux, S. Iwata, A. Rogalev, and J. Goulon, J. Electron Spectrosc. Relat. Phenom. **92**, 35 (1998).
[95] C. G. Shull and M. K. Wilkinson, Phys. Rev. **97**, 304 (1955).
[96] Yu. A. Dorofeyef, A. Z. Men'shikov, and S. K. Sidorov, Fiz. Met. Metalloved. **40**, 978 (1975).
[97] R. Coehoorn, J. Magn. Magn. Mater. **55**, 159 (1996).
[98] Yu. A. Dorofeyev, A. Z. Men'shikov, and S. K. Sidorov, Fiz. Met. Metalloved. **40**, 1178 (1975).
[99] R. Wirths, P. Runow, and H. W. Schopgens, Phys. Status Solidi A **33**, 135 (1976).
[100] K. Mikke, V. A. Udovenko, J. K. Milczavek, E. Z. Vintaikin, S. Y. Makushev, and V. B. Dmitriev, J. Phys. (Paris) **49**, C8-185 (1988).
[101] A. Kjekshus, R. Möllerud, A. F. Andresen, and W. B. Pearson, Philos. Mag. **16**, 1063 (1967).
[102] K. Kren, E. Nagy, L. Pal, and P. Szabo, J. Phys. Chem. Solids **29**, 101 (1968).
[103] J. M. Sanchez, J. L. Moran-Lopez, C. Leroux, and M. C. Cadeville, J. Phys. (Paris) **49**, C8-107 (1988).
[104] Y. Nakagawa and T. Hori, J. Phys. Soc. Jpn. **19**, 2082 (1964).